The sulfur-related metabolic status of *Aspergillus fumigatus* during infection reveals cytosolic serine hydroxymethyltransferase as a promising antifungal target.

In vivo transcriptomics to identify new antifungal targets and validation of SHMT

Reem Alharthi[1], Monica Sueiro-Olivares[1], Isabelle Storer[1], Hajer Alshammri[1], Jennifer Scott[1], Reem Al-Shidhani[2], Rachael Fortune-Grant[1], Elaine Bignell[3], Lydia Tabernero[2], Michael Bromley[1], Can Zhao[4], and Jorge Amich[1,5]*

1. Manchester Fungal Infection Group (MFIG), Division of Evolution, Infection, and Genomics, Faculty of Biology, Medicine and Health, University of Manchester, Manchester, M13 9PT UK.
2. School of Biological Sciences, Faculty of Biology Medicine and Health, Manchester Academic Health Science Centre, University of Manchester, Manchester M13 9PT, UK
3. MRC Centre for Medical Mycology, University of Exeter, Exeter, United Kingdom.
4. Department of Life Sciences, Manchester Metropolitan University, Manchester, M1 5GD, United Kingdom.
5. Mycology Reference Laboratory (Laboratorio de Referencia e Investigación en Micología LRIM), National Centre for Microbiology, Instituto de Salud Carlos III (ISCIII), Majadahonda, 28220 Madrid, Spain.

*Correspondence to Jorge Amich: jamich@isciii.es

ABSTRACT

Sulfur metabolism is an essential aspect of fungal physiology and is known to be crucial for pathogenicity. Fungal sulfur metabolism comprises anabolic and catabolic routes that are not well-conserved in mammals, and therefore can be considered a promising source of prospective novel antifungal targets. To gain insight into the status of the *Aspergillus fumigatus* sulfur-related metabolism during infection we used a NanoString custom nCounter TagSet and compared the expression of 68 key metabolic genes in different murine models of invasive pulmonary aspergillosis, at three different time-points, and a variety of *in vitro* conditions. We identified a set of 15 genes that are consistently expressed at higher levels *in vivo* than *in vitro*, suggesting that they may be particularly relevant for intrapulmonary growth and therefore constitute promising drug targets. Indeed, the role of five of the fifteen genes had previously been empirically validated, supporting the likelihood that the remaining candidates are relevant. In addition, the analysis of the dynamics of gene expression at the early (16h), mid (24h) and late (72h) time-points uncovered potential disease initiation and progression factors. We further characterised one of the identified genes, encoding the cytosolic serine hydroxymethyltransferase ShmB, and demonstrated that it is an essential gene of *A. fumigatus* and that it is also required for virulence in a murine model of established pulmonary infection. We further show that the structure of the ligand binding pocket of the fungal enzyme differs significantly from its human counterpart, suggesting that specific inhibitors can be designed. Therefore, *in vivo* transcriptomics is a powerful tool to identify genes crucial for fungal pathogenicity that might encode promising antifungal target candidates.

AUTHOR SUMMARY

Aspergillus fumigatus is an opportunistic human fungal pathogen that causes devastating chronic and invasive infections in immunocompromised patients. Our arsenal of antifungal drugs to fight this and other fungal pathogens is very limited, partly because of the high similarity between eukaryotic fungal and human cells makes the identification of suitable drug targets a challenging task. Furthermore, targets identified *in vitro* are often not effective *in vivo*, as their action is not relevant for fungal virulence. To address this challenge, we compared the expression profiles of a set of genes involved in sulfur metabolism, a promising source of potential drug targets, in numerous *in vitro* and *in vivo* conditions to identify favourable antifungal candidates. Subsequently, we validated one of the highlighted genes, demonstrating that it is essential for *A. fumigatus* viability and virulence, and that it can likely be targeted by specific inhibitors. Hence, we show the potential of using *in vivo* transcriptomics to identify targets that contribute to virulence, propose various candidates for future studies and present a novel target validated for further antifungal drug development.

63 **INTRODUCTION**

64 *Aspergillus fumigatus* is a ubiquitous mould that normally lives in the soil feeding on decaying organic
65 matter [1]. During its natural life-cycle *A. fumigatus* produces thousands of spores, also known as
66 conidia, that are disseminated in the air. Because of their high abundance and prevalence, it has been
67 estimated that every human breathes in several hundred of these conidia on a daily basis [2] and, due
68 to their small size (2-3 µm), they have the potential to penetrate deep into the respiratory tract and
69 even reach the lung alveoli [3]. In immunocompetent individuals, this has no consequence as epithelial
70 mucocilliarity and a proper immune response eliminate the spores very efficiently [4]. However,
71 patients with an imbalanced immune response are susceptible to *A. fumigatus*, which can cause a
72 wide range of diseases collectively termed aspergilloses [5]. Chronic and invasive aspergilloses are life-
73 threatening infections with high mortality rates, even in patients under antifungal treatment [6, 7].
74 First line therapy against aspergilloses is based on the use of azoles, the only class of antifungals that
75 can be orally administered. Worryingly, the number of clinical *A. fumigatus* isolates that are resistant
76 to triazole antifungals is increasing worldwide, which correlates with higher mortality rates [6, 8, 9].
77 Consequently, new agents to fight this fungal pathogen are urgently required.

78 Metabolism is central to the virulence of fungal pathogens, and therefore its targeting is considered a
79 promising strategy for the development of novel antifungals [10, 11]. Fungal sulfur metabolism is
80 particularly interesting as it comprises routes and enzymes that are often not conserved in humans,
81 and thus it is considered a propitious source of novel antifungal targets [12]. Indeed, we have
82 previously shown that a proper regulation of sulfur metabolism is crucial for *A. fumigatus* infective
83 capacity [13], demonstrated that biosynthesis of the S-containing amino acids is required for virulence
84 [14], and comprehensively characterised an enzyme in the trans-sulfuration pathway, methionine
85 synthase, as a promising antifungal target [15]. Others have also shown that sulfur is involved in the
86 biosynthesis of essential fungal metabolites [16] and proposed sulfur assimilation and the trans-
87 sulfuration pathway as sources of antifungal targets [17, 18]. Here, we aimed to expand on that
88 knowledge by using *in vivo* transcriptomics to better characterise the fungal sulfur metabolic status
89 during infection of the murine lung, and to use the expression profile of genes to identify those that
90 may be relevant for infection, proposing them as promising candidates for further investigations.
91 However, detection and analysis of the fungal transcriptome during infection is a persistent challenge,
92 as fungal RNA usually represents only between 0.05 and 0.5% of the total RNA isolated from infected
93 organs [19]. To overcome this obstacle, we have used NanoString nCounter, a novel probe-based
94 technology with excellent reproducibility, sensitivity, and specificity when compared to other
95 transcriptomic methods such as microarray hybridisation or RT-qPCR [20, 21]. Its high sensitivity, being
96 capable of detecting mRNA concentrations in the femtomolar range [22], makes this technology ideal

97 for detecting and quantifying fungal RNA during infection. Furthermore, its incomparable specificity is
98 fundamental to prevent any crosstalk with the abundant host RNA. Using this technology, we have
99 assessed the transcription profile of a selection of metabolic genes during infection of the murine lung
100 in two models of immunosuppression and at three time-points post infection, and compared them
101 with the expression profiles under a variety of *in vitro* conditions. By these means we have uncovered
102 interesting aspects of the *in vivo* sulfur metabolic status and identified genes that can be proposed as
103 relevant for growth in the tissues. We have further characterised a promising candidate, the cytosolic
104 serine hydroxymethyltransferase (*shmB*) encoding gene, demonstrating that it is essential for *A.*
105 *fumigatus* viability as well as for virulence and that it is promising to aim for the development of
106 fungal-specific inhibitors against this target, which can serve to address the emerging global threat of
107 antifungal resistance [23, 24].

108

109 **RESULTS**

110 *Linear amplification of Aspergillus fumigatus mRNAs allows gene expression profiling of low input in*
111 *vivo samples.*

112 To determine the transcriptional status of genes related to sulfur metabolism during fungal infection
113 of the murine lung, we developed a custom NanoString nCounter Elements TagSet comprising 68
114 metabolic genes (51 directly related to S-metabolism and 17 metabolic genes of interest indirectly
115 related with S-metabolism) and 4 housekeeping controls (Table S1). We isolated RNA from *A.*
116 *fumigatus* propagated under a variety of *in vitro* conditions (Table S2) and from the lungs of infected
117 mice immunosuppressed with two different regimens, the leukopenic and the corticosteroid model
118 (Table S2 and see material and methods). We isolated the lungs of infected mice at three different
119 time-points to investigate gene expression at an early (16h), medium (24h) and late (72h) time point
120 of infection (3 mice per time-point). We further assayed a chronic model of pulmonary aspergillosis
121 [25] to determine if this model provides a significantly different S-environment (Table S2). A
122 preliminary experiment revealed that fungal RNA could not be reliable detected at 16h and 24h post-
123 infection, which is expected as the fungal burden at those early times is very low. To circumvent this
124 problem, we applied the Nanostring Single Cell Gene Expression protocol (see Material and Methods)
125 to perform linear amplification using Multiplexed Target Enrichment (MTE) primers. To verify that the
126 MTE enrichment does not affect the relative abundance of transcripts, we compared the fold changes
127 between diluted-amplified and non-amplified (undiluted) *in vitro* (-S limiting conditions) and *in vivo*
128 samples (lungs extracted from two leukopenic mice 72h after infection) (Fig 1A). This direct
129 comparison demonstrated that the correlation of the fold changes detected with non-amplified and

130 amplified samples was very high (R^2=0.95 for mouse 1 and R^2=0.84 for mouse 2). Therefore, MTE
131 enrichment of low input fungal RNA samples does not affect the relative abundance of transcripts and
132 can be used to investigate gene expression in the mammalian lung at early time-points after infection.

133

Fig. 1

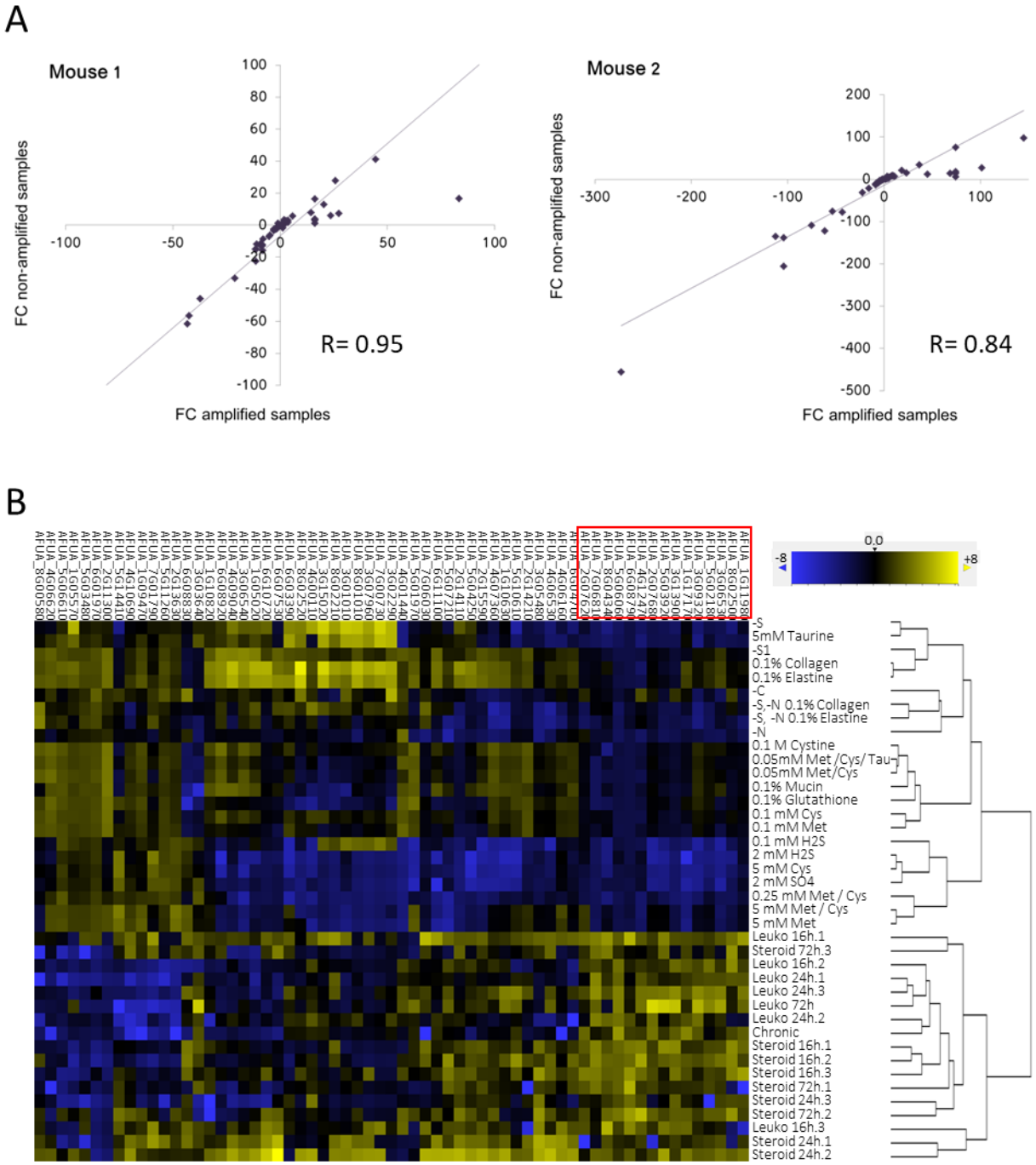

134

135 **Figure 1. Identification of genes potentially relevant *for Aspergillus fumigatus* virulence using**
136 **NanoString *in vivo* transcriptomics.**

137 **A)** Validation of the linear amplification performed with the Nanostring Single Cell Gene Expression
138 protocol with Multiplexed Target Enrichment (MTE) primers. The fold changes between diluted-
139 amplified and non-amplified (undiluted) *in vitro* (-S limiting conditions) and *in vivo* samples (lungs
140 extracted from two leukopenic mice 72h after infection) were compared. For both mice, there was a
141 linear relationship between the FCs of non-amplified and amplified samples, demonstrating that
142 amplification did not affect the relative abundance of transcripts. **B)** Hierarchical clustering of all
143 samples formed two distinct branches, one of *in vitro* samples and one with the *in vivo* samples. There
144 were 15 genes (red line) that were always expressed at higher levels in the *in vivo* samples, compared
145 with all the *in vitro* samples.

146

147 *The fungal S-related metabolic status in vivo is different from that of in vitro conditions, revealing*
148 *genes potentially relevant for infection*

149 To analyse the S-related fungal metabolic status *in vivo* and *in vitro*, we hybridized and read our
150 custom NanoString codeset with isolated RNAs or amplified cDNAs (Table S2). The obtained raw data
151 was subjected to quality control, which revealed that the samples obtained from two leukopenic mice
152 72h had not run properly: they were borderline for the recommended threshold of overall number of
153 counts (10,000) and did not reach the minimum values for the positive counts reads (Fig. S1A and S1B).
154 Consequently, these samples were excluded from all analyses. In addition, inspection of the
155 normalized data (see Material and Methods for details) revealed that five genes (AFUA_3G06492,
156 AFUA_1G06940, AFUA_5G08600, AFUA_4G03950 and AFUA_6G00760) had a very low number of
157 counts (<20) in all samples. This could be due to the genes not being expressed at all or at very low
158 levels in the tested conditions, or to failure of the NanoString designed probes to detect these mRNAs.
159 Accordingly, these genes were also excluded from all downstream analyses.

160 We first performed a hierarchical clustering of all samples analysed (Fig. 1B). By this stratification, the
161 *in vivo* samples clearly clustered separately from the *in vitro* samples, indicating that the fungal S-
162 related metabolic status during infection is significantly different from that during growth in diverse
163 experimental conditions This suggests that the lung provides a unique environment in terms of sulfur
164 metabolism that is distinct from defined culture media. Based on this, we hypothesised that genes
165 which are consistently more highly expressed *in vivo*, compared to in the great variety of tested *in*
166 *vitro* conditions, may be particularly relevant for the fungal capacity to grow in the lung tissues, and

167 therefore for fungal virulence. We detected 15 genes which were always expressed more *in vivo* than
168 *in vitro* (Fig. 1B, red box, Table 1). Interestingly, we and others have already demonstrated the
169 importance of at least five of those genes for *A. fumigatus* virulence, and a further six genes had
170 already been proposed to be potentially relevant (Table 1 and see discussion), supporting the rationale
171 that the uncharacterized genes might be valid candidates for further analyses.

GENE ID	DESCRIPTION	VIRULENCE
AFUA_1G11980	Glutamine amidotransferase (HisfF/H)	Suspected [26]
AFUA_8G02500	Glutathione S-transferase	Suspected [27]
AFUA_3G06530	ATP sulfurylase (sC)	Unknown
AFUA_5G02180	Cysteine synthase (CysB)	Proven [14]
AFUA_3G09320	Serine hydroxymethyltransferase (SmhB)	This work
AFUA_1G17170	Taurine dioxygenase	Unknown
AFUA_3G13900	Glutamate-cysteine ligase (Gcs1)	Suspected [27]
AFUA_5G03920	bZIP transcription factor (HapX)	Proven [28]
AFUA_2G07680	L-ornithine N5-oxygenase (SidA)	Proven [29]
AFUA_4G12470	bZIP transcription factor (CpcA)	Proven [30]
AFUA_6G08790	C6 transcription factor (PrnA)	Unknown
AFUA_5G06060	SCF-complex subunit (SkpA)	Suspected [31, 32]
AFUA_8G04340	cystathionine gamma-lyase (MecB)	Proven [33]
AFUA_7G06810	L-amino acid oxidase (LaoA)	Suspected [34]
AFUA_2G07620	Cystathionine beta-synthase (mecA)	Suspected [33]

172

173 **Table 1.** Genes that consistently showed higher expression *in vivo* compared to any of the tested *in*
174 *vitro* conditions.

175

176

177 *Fungal sulfur related in vivo metabolism is influenced by the model of immunosuppression and the*
178 *course of infection.*

179 To investigate if the fungal S-related metabolic status is influenced by the model of
180 immunosuppression, we performed hierarchical clustering of all the *in vivo* samples (Fig. 2A). This
181 clustering showed that the fungal S-related status is quite variable *in vivo* (notice that the dynamic
182 range of expression are much smaller than when comparing *in vitro* and *in vivo* samples in Fig. 1B),
183 and is partially dependent on the model of immunosuppression, as 5 out of the 8 leukopenic mice
184 aggregated in a separated cluster. Interestingly, the chronic model clustered in this separated branch,
185 suggesting that the fungal S-related metabolic status in this type of infection is more similar to the
186 status in the leukopenic model than in the steroid-induced one. Nevertheless, some samples from
187 leukopenic mice interleaved with the samples from steroid-treated mice, demonstrating that the
188 model of immunosuppression is not the only factor that determines the fungal metabolic status.

189 To investigate to what extent the fungal S-related metabolic status is influenced by the course of
190 infection, we performed hierarchical clustering of the samples from leukopenic and steroid-treated
191 mice separately (Fig 2B). In both models of suppression there was a partial aggregation of samples
192 according to the time point post infection, suggesting that the course of infection is mirrored by the
193 S-related metabolic status of the fungal pathogen.

194 In conclusion, the model of immunosuppression as well as the time of duration of infection appear to
195 influence the status of the fungal S-related metabolism. However, these variables alone or combined
196 cannot explain the variances among samples, indicating that other factors must be involved. For
197 instance, it is to be expected that the exact anatomic location of the foci of fungal growth would
198 account for different microenvironments that in turn affect the fungal S-related metabolism.

199

Fig. 2

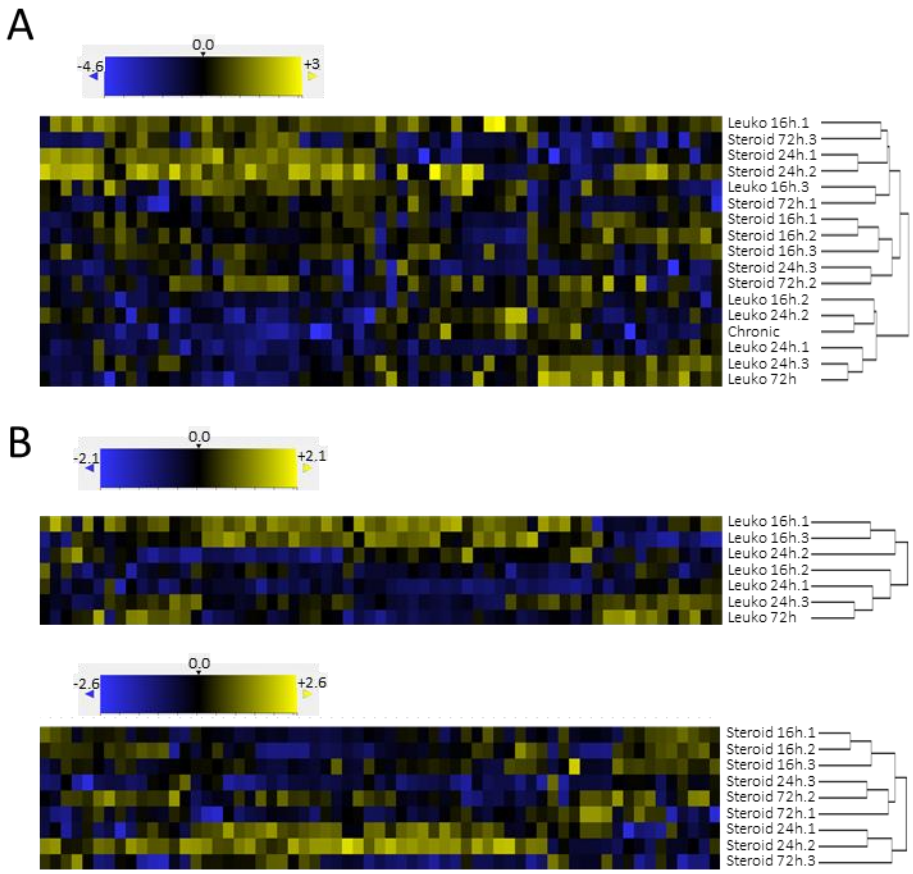

200

201

202 **Figure 2. The fungal S-related sulfur metabolism *in vivo* is influenced by the model of suppression**
203 **and the time of infection.**

204 **A)** Hierarchical clustering of all *in vivo* samples created two major branches, one almost exclusive for
205 leukopenic samples, which only included the chronic model sample. The second major branch was
206 divided again in two branches, one exclusive for steroid samples and the other mixed with leukopenic
207 and steroid samples. Therefore, the model of suppression influences but is not the only factor that
208 determines the fungal metabolic status. **B)** Separated hierarchical clustering of leukopenic or steroid
209 samples partially aggregated by the time of infection. Therefore, the fungal S-related metabolism is
210 influenced *in vivo* by the status of infection.

211

212 *Temporal dynamics of gene expression in vivo versus in vitro reveals the existence of potential disease*
213 *initiation and progression factors*

214 Since we found that the S-related metabolic status correlates with the time period post infection, we
215 reasoned that some genes may be expressed at different levels as the fungal infection progresses. To
216 investigate this hypothesis, we first examined the fold change of the (geometric) mean expression of
217 all genes in each time-point with respect to the corresponding 16h condition (Fig. 3A). This analysis
218 revealed that indeed many genes change the level of expression during the course of infection:
219 transcription of several genes seemed to consistently increase, a few decreased expression as
220 infection progressed, and some appeared to increase or decrease expression at mid-infection (24h)
221 before returning to initial levels in late infection (72h). To explore whether any of these genes that
222 show temporal dynamic expression could be particularly important for *in vivo* growth, we analysed
223 the fold change of all genes in each *in vitro* condition versus each of the leukopenic (Fig. 3B) or steroid-
224 treated (Fig. 3C) samples grouped by the time after infection. As expected, we identified some genes
225 which showed a temporal variance *in vivo* compared with *in vitro*. In detail, in leukopenic mice we
226 observed that genes *metAT* (AFUA_2G13630), *cdoB* (AFUA_5G14410), *cysAT* (AFUA_1G09470) and
227 *isa1* (AFUA_4G10690) had higher transcript levels *in vivo* at early (16h) than at mid (24h) or late (72h)
228 time points after infection (Fig. 3B orange box), suggesting that these genes may be particularly
229 important for the initiation of infection, but possibly not as relevant for progression and maintenance
230 of infection. In contrast, *cdoA* (AFUA_1G05570) had higher *in vivo* transcription during advanced
231 infection (Fig. 3B, dark blue box), suggesting that this gene may be relevant for growth in progressively
232 invaded tissue. The genes *hisB* (AFUA_6G04700), *sD* (AFUA_1G10820), *metR* (AFUA_4G06530) and
233 *hapX* (AFUA_5G03920) displayed higher expression at early (16h) and late (72h) time after infection
234 (Fig. 3B, purple box), suggesting that they may be particularly important to initiate infection and during

235 established infection, but that they are not crucial for infection to progress. Similarly, in steroid treated
236 mice, we observed that genes *sFα* (AFUA_6G08920), *sB* (AFUA_1G05020), *sA* (AFUA_3G06540), *mupA*
237 (AFUA_4G09040), *mupB* (AFUA_7G00730), *sfnB* (AFUA_8G01010), two taurine dioxygenase encoding
238 genes (AFUA_3G0796 and AFUA_3G01010) and one arylsulfatase encoding gene (AFUA_8G02520)
239 had higher expression *in vivo* at mid-infection time (24h) (Fig. 3C, orange boxes), suggesting that these
240 genes may play a role in this model for the progression of infection. Finally, genes *metAT*
241 (AFUA_2G13630), *cysAT* (AFUA_1G09470), *isa1* (AFUA_4G10690) and *ssuA* (AFUA_7G01790) had
242 higher expression at mid- (24h) and late (72h) times after infection (Fig. 3C, purple box), indicating
243 that they may be more relevant for progression and maintenance of infection than for its initiation.

244 We therefore propose that the temporal dynamics of *in vivo* transcript levels may be useful to identify
245 and differentiate fungal factors of disease initiation and progression, defined as products that are
246 essential for the initiation of infection or that facilitate persistence and continued disease progression
247 [35]. Although this hypothesis needs to be validated further by confirming the role of some of our
248 identified candidates as true disease initiation or progression factors in appropriate models of
249 infection, we emphasise the potential of *in vivo* transcriptomics at distinct stages of infection to detect
250 such initiation and progression factors, as has already been proposed [35].

251

252

253

254

255

256

257

258

259

260

261

262

263

Fig. 3

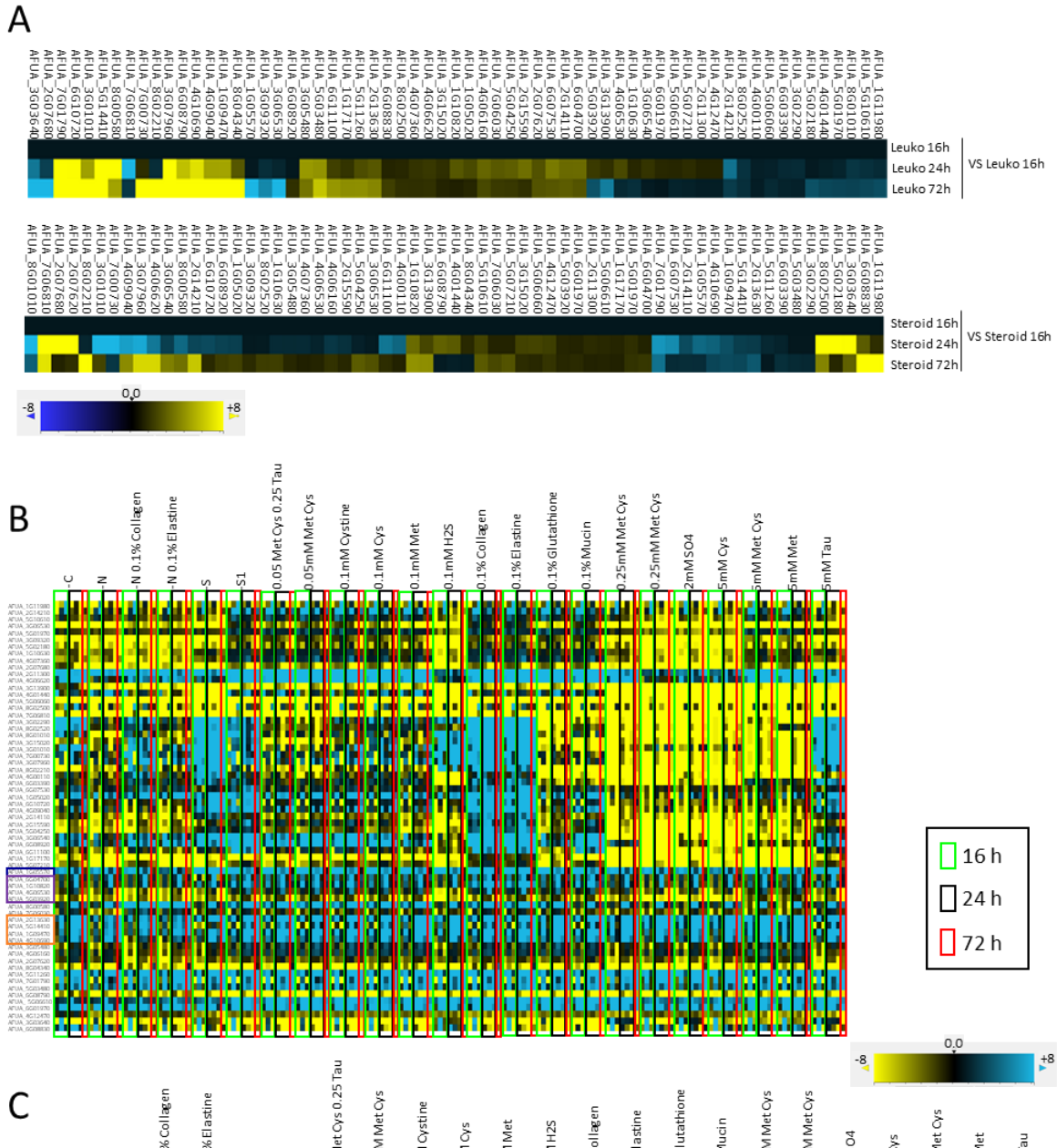
A
Leuko 16h
Leuko 24h
Leuko 72h
VS Leuko 16h
Steroid 16h
Steroid 24h
Steroid 72h
VS Steroid 16h
-8
0,0
+8
B
-C
-N
-N 0.1% Collagen
-N 0.1% Elastine
-S
-S1
0.05 Met Cys 0.25 Tau
0.05mM Met Cys
0.1mM Cystine
0.1mM Cys
0.1mM Met
0.1mM H2S
0.1% Collagen
0.1% Elastine
0.1% Glutathione
0.1% Mucin
0.25mM Met Cys
0.25mM Met Cys
2mM SO4
5mM Cys
5mM Met Cys
5mM Met
5mM Tau
16 h
24 h
72 h
-8
0,0
+8
C
-C
-N
-N 0.1% Collagen
-N 0.1% Elastine
-S
-S1
0.05 Met Cys 0.25 Tau
0.05mM Met Cys
0.1mM Cystine
0.1mM Cys
0.1mM Met
0.1mM H2S
0.1% Collagen
0.1% Elastine
0.1% Glutathione
0.1% Mucin
0.25mM Met Cys
0.25mM Met Cys
2mM SO4
5mM Cys
5mM Met Cys
5mM Met
5mM Tau

265 **Figure 3. Temporal dynamics of gene expression reveals the existence of potential initiation and**
266 **disease progression factors.**

267 **A)** Fold change of expression of genes in each time-point with respect to the correspondent 16h
268 condition revealed that most genes changed expression during the course of infection The geometric
269 mean value for each time-point was used. **B)** Fold change of all genes in each *in vitro* condition versus
270 each of the leukopenic samples ordered by the time after infection identified temporal dynamics in
271 the expression of certain genes. Four genes showed higher expression *in vivo* at 16h than at 24h and
272 72h after infection (orange box). One gene had had higher expression *in vivo* at 72h time (red arrow).
273 Four genes had higher expression at 16h and 72h time after infection (purple box). **C)** Fold change of
274 all genes in each *in vitro* condition versus each of the steroid-treated samples ordered by the time
275 after infection identified temporal dynamics in the expression of certain genes. Nine genes had higher
276 expression *in vivo* at 24h (orange boxes). Four genes showed higher expression at 24h and 72h after
277 infection (purple box). Samples for 16h are clustered in green rectangles, for 24h in black rectangles
278 and for 72h in red rectangles.

279

280 *Validation of an identified gene, encoding a serine hydroxymethyltransferase (SHMT), as a promising*
281 *target for antifungal drug development.*

282 To demonstrate the value of the NanoString technology in identifying genes relevant for *A. fumigatus*
283 virulence, and aiming to validate a novel drug target, we decided to further investigate the serine
284 hydroxymethyltransferase encoding gene (*shmB,* AFUA_3G09320), which was consistently expressed
285 at higher levels *in vivo* compared with *in vitro* conditions (Fig. 1B). *A. fumigatus* genome encodes two
286 paralogues of serine hydroxymethyltransferase, ShmA (annotated as AFUA_2G07810, not included in
287 the NanoString analysis) and ShmB. The ShmB protein contains 471 amino acids (aa) and ShmA is 537
288 aa in length, and both share an identity of 61.9% and similarity of 79.9% (Fig. 4A). Interestingly, ShmA
289 has a long N-terminus region that is absent in ShmB (Fig. 4A), which prompted us to investigate the
290 subcellular localisation of the proteins using three different public softwares: DeepMito [36], PProwler
291 [37], and TargetP [38]. In contrast to the current annotation in FungiDB and NCBI databases, all three
292 algorithms predicted a mitochondrial localisation for ShmA and a cytosolic for ShmB. Indeed, when
293 we aligned the *A. fumigatus* proteins with their *Saccharomyces cerevisiae* orthologues, we observed
294 that the yeast mitochondrial enzyme SHM1 also had a longer N-terminus in comparison to the
295 cytosolic proteins (Fig. S2A).

296 Therefore, aiming to clarify the subcellular localisation of ShmA and ShmB in *A. fumigatus* we tagged
297 the proteins at their C-terminus with the fluorescent YFP-derivative Citrine to express them under the
298 control of their native promoters. In line with our predictions, we found that the ShmB-Citrine protein
299 localises throughout the cytoplasm, with a similar pattern to a control strain that expresses Citrine
300 under the control of the strong *gdpA* promoter (Fig. 4B). Regrettably, ShmA-Citrine could not be
301 detected, possibly reflecting very low or no expression of the encoding gene under steady-state
302 conditions, which would be supported by its dispensability under standard laboratory conditions (see
303 below).

304 To investigate the potential relevance of ShmA and ShmB for fungal virulence, we initially attempted
305 to construct single null mutants deleted for each encoding gene. We successfully constructed a *ΔshmA*
306 mutant, which showed no phenotype on regular laboratory conditions, growing perfectly on rich
307 Sabouraud and defined AMM media (Fig. S2B). In contrast, we were unable to generate a *ΔshmB*
308 mutant, suggesting that this might be an essential gene in *A. fumigatus*. We therefore constructed
309 two mutant strains in which we placed the *shmB* coding region under the control of the *tetOFF* module
310 [39, 40], one in the wild-type background and one in the *ΔshmA* background. The *tetOFF* system allows
311 downregulation of transcription of the gene of interest, in this case *shmB*, upon supplementation of
312 doxycycline (Dox) [39]. Addition of Dox inhibited growth of both strains (*shmB_tetOFF* and *ΔshmA-*
313 *shmB_tetOFF*) on AMM solid plates (Fig. 4C), proving that *shmB* is essential for viability independently
314 of its paralogue *shmA*. Gene essentiality is a conditional phenomenon, whereby particular
315 growth/environmental conditions may overcome the disturbances derived from the gene deficiency
316 [40-43]. Therefore, we attempted to reconstitute growth of the *shmB_tetOFF* strain in the presence
317 of Dox by supplementing compounds that could potentially be depleted in the absence of ShmB (Fig.
318 4D). We have previously observed that disturbances in the folate cycle causes a need of amino acid
319 supplementation [44], therefore, we assayed all phenotypic conditions on AMM without nitrogen
320 (AMM-N, to diversify and increase the presence of permeases in the membrane that ensure uptake
321 of amino acids and other compounds) supplemented with 1 mg/mL of all proteinogenic amino acids.
322 Additionally, we tried to reconstitute growth by supplementing the media with 5,10-
323 methylenetetrahydrofolate (CH_2-THF) and glycine (separately and combined), or with folic acid and
324 serine (substrates/products of the bidirectional enzymatic reaction), or with adenine (as blockade of
325 the folate cycle might impair purine biosynthesis [45]). In addition, we tested adding ATP to all those
326 supplements, as we previously showed that impairing the folate cycle *via* blocking the activity of
327 methionine synthase impacts cellular energetics in *A. fumigatus* [40]. The only condition that could
328 partly reconstitute growth, albeit not to wild-type levels, was supplementation with adenine and ATP
329 (Fig. 4D). None of the supplement combinations reconstituted growth of the *shmB_tetOFF* strain

330 under restrictive conditions (Fig. 4D). Therefore, either *shmB* is a truly essential gene, or the conditions
331 to overcome its essentiality are complex and yet unknown. Yet, based on these results *shmB*
332 constitutes a promising drug target candidate, and consequently we decided to test its value in an *in*
333 *vivo* infection model.

334 We have recently proposed that potential drug targets should be validated in models of established
335 infection, which is particularly relevant for essential genes (to confirm that essentiality cannot be
336 overcome during active growth in the host tissues) [40]. Therefore, we assayed our optimised protocol
337 to investigate targets in established *A. fumigatus* invasive pulmonary infections with the *tetOFF*
338 system [40]. Initially, we confirmed that Dox addition very strongly turns down *shmB* expression in
339 growing mycelium (Fig. S2C). Next, we infected leukopenic mice with 2×10^5 conidia of the
340 *shmB_tetOFF* strain, started Dox treatment 16h after infection and measured fungal burden in the
341 lungs 72h after infection. As control we also infected mice with the previously validated strain
342 *Δcyp51B-cyp51A-tetOFF* [40], which expresses *cyp51A*, the gene that encodes the target of the azole
343 antifungals, under the control of the same *tetOFF* system. Therefore, this control strain serves to
344 corroborate that downregulating a validated target (azoles are the gold standard therapy for invasive
345 pulmonary aspergillosis) causes a significant reduction in fungal burden, as indeed we detected (Fig.
346 4E). Interestingly, we found that downregulation of *shmB* in the established infection model triggered
347 a significant reduction in fungal burden (Fig. 4E). Hence, ShmB appears to be a valid target for the
348 treatment of aspergillosis infections.

349

350

351

352

353

354

355

356

357

358

359

Fig. 4

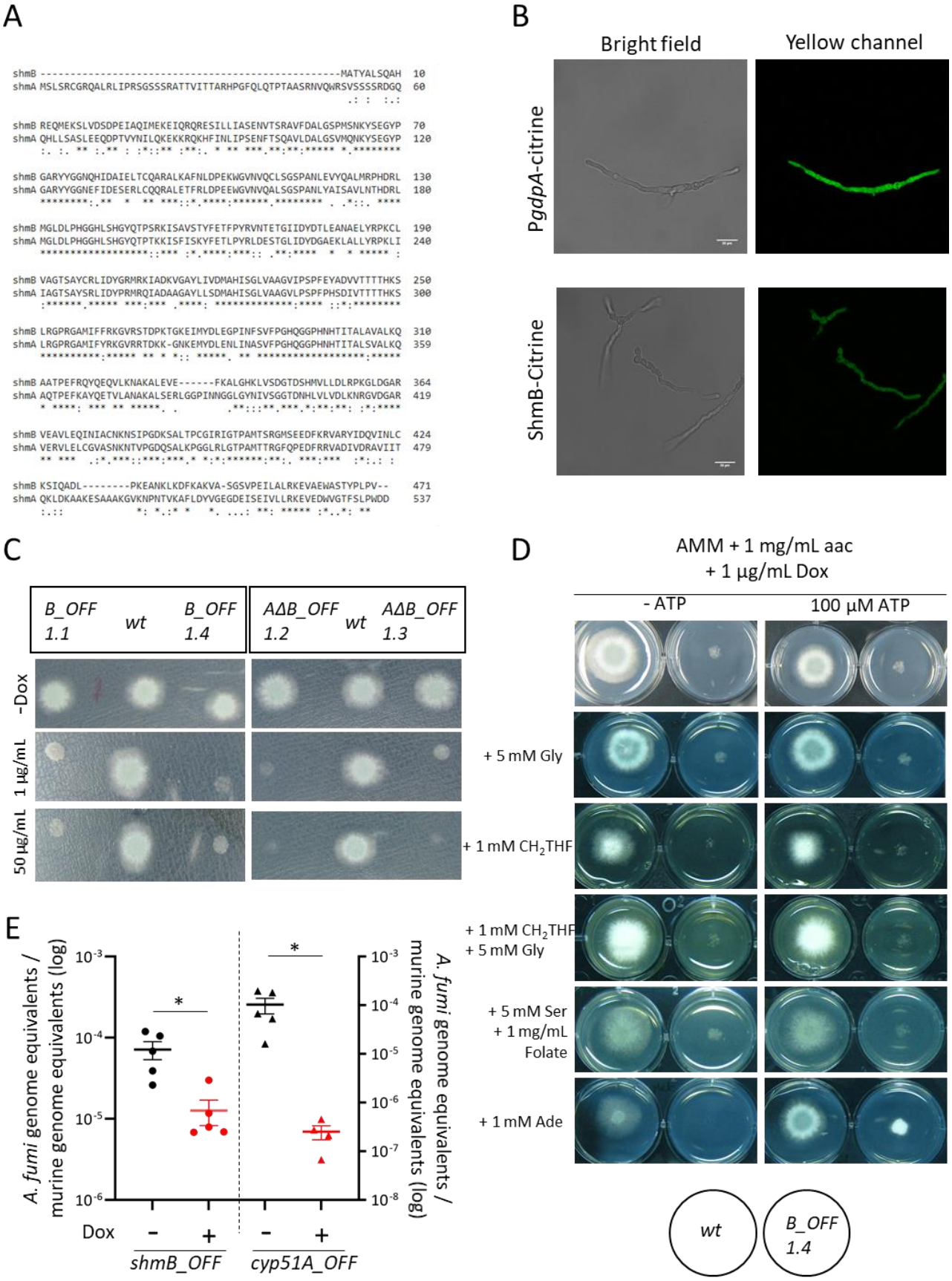
A
shmB ----------MATYALSQAH 10
shmA MSLSRCGRQALRLIPRSGSSSRATTVITTARHPGFQLQTPTAASRNVQWRSVSSSSRDGQ 60
shmB REQMEKSLVDSDPEIAQIMEKEIQRQRESILLIASENVTSRAVFDALGSPMSNKYSEGYP 70
shmA QHLLSASLEEQDPTVYNILQKEKKRQKHFINLIPSENFTSQAVLDALGSVMQNKYSEGYP 120
shmB GARYYGGNQHIDAIELTCQARALKAFNLDPEKWGVNVQCLSGSPANLEVYQALMRPHDRL 130
shmA GARYYGGNEFIDESERLCQQRALETFRLDPEEWGVNVQALSGSPANLYAISAVLNTHDRL 180
shmB MGLDLPHGGHLSHGYQTPSRKISAVSTYFETFPYRVNTETGIIDYDTLEANAELYRPKCL 190
shmA MGLDLPHGGHLSHGYQTPTKKISFISKYFETLPYRLDESTGLIDYDGAEKLALLYRPKLI 240
shmB VAGTSAYCRLIDYGRMRKIADKVGAYLIVDMAHISGLVAAGVIPSPFEYADVVTTTTHKS 250
shmA IAGTSAYSRLIDYPRMRQIADAAGAYLLSDMAHISGLVAAGVLPSPFPHSDIVTTTTHKS 300
shmB LRGPRGAMIFFRKGVRSTDPKTGKEIMYDLEGPINFSVFPGHQGGPHNHTITALAVALKQ 310
shmA LRGPRGAMIFYRKGVRRTDKK-GNKEMYDLENLINASVFPGHQGGPHNHTITALSVALKQ 359
shmB AATPEFRQYQEQVLKNAKALEVE------FKALGHKLVSDGTDSHMVLLDLRPKGLDGAR 364
shmA AQTPEFKAYQETVLANAKALSERLGGPINNGGLGYNIVSGGTDNHLVLVDLKNRGVDGAR 419
shmB VEAVLEQINIACNKNSIPGDKSALTPCGIRIGTPAMTSRGMSEEDFKRVARYIDQVINLC 424
shmA VERVLELCGVASNKNTVPGDQSALKPGGLRLGTPAMTTRGFQPEDFRRVADIVDRAVIIT 479
shmB KSIQADL--------PKEANKLKDFKAKVA-SGSVPEILALRKEVAEWASTYPLPV-- 471
shmA QKLDKAAKESAAAKGVKNPNTVKAFLDYVGEGDEISEIVLLRKEVEDWVGTFSLPWDD 537
B
Bright field
Yellow channel
PgdpA-citrine
ShmB-Citrine
C
B_OFF 1.1
wt
B_OFF 1.4
AΔB_OFF 1.2
wt
AΔB_OFF 1.3
-Dox
1 µg/mL
50 µg/mL
D
AMM + 1 mg/mL aac
+ 1 µg/mL Dox
- ATP
100 µM ATP
+ 5 mM Gly
+ 1 mM CH2THF
+ 1 mM CH2THF
+ 5 mM Gly
+ 5 mM Ser
+ 1 mg/mL
Folate
+ 1 mM Ade
wt
B_OFF
1.4
E
A. fumi genome equivalents / murine genome equivalents (log)
10-3
10-4
10-5
10-6
10-7
10-8
*
Dox
-
+
shmB_OFF
cyp51A_OFF

360

361 **Figure 4. The cytosolic serine hydroxymethyltransferase is essential for viability and virulence in**
362 ***Aspergillus fumigatus***.

363 **A)** Alignment of the amino acid sequences of the two serine hydroxymethyltransferase enzymes
364 encoded in *A. fumigatus* genome. The proteins have 61.9% identity and 79.9% similarity. ShmA has a
365 long N-terminus region that is absent in ShmB and which after further analysis (see text) suggests that
366 ShmA is mitochondrial. **B)** A ShmB-Citrine tagged proteins localised diffused throughout the
367 cytoplasm, similarly as the control P*gdpA*-Citrine strain. **C)** A Phenotypic assay with two independent
368 clones of the *shmB_tetOFF* and *ΔshmA shmB_tetOFF* mutant strains. In the presence of doxycycline
369 (Dox) the mutants did not grow, demonstrating that *shmB* is essential in *A. fumigatus*, and that ShmA
370 cannot cover its function. Plates were incubated for 48 h at 37 °C. the experiment was repeated twice
371 independently. **D)** Attempting to reconstitute *shmB_tetOFF* growth in restrictive conditions (+Dox),
372 media was supplemented with various metabolites which could potentially be limited in the absence
373 of serine hydroxymethyltransferase activity. The only condition that could partly reconstitute growth,
374 not at wild-type level, was supplementation with ATP and adenine (Ade). Plates were incubated for
375 48 h at 37 °C. The experiment was repeated twice independently. **E)** Fungal burden in the lungs of
376 leukopenic mice treated or untreated with Dox. Downregulation of *cyp51A* (encoding the target of the
377 azoles) expression caused a significant reduction in burden (p=0.0159 in a nonparametric Mann
378 Whitney test and p=0.0476 in an unpaired t-test with Welch's correction). Similarly, downregulation
379 of *shmB* triggered a significant decrease in fungal burden (p=0.0159 in a nonparametric Mann Whitney
380 test and p=0.0288 in an unpaired t-test with Welch's correction). Therefore, ShmB appears to be a
381 valid antifungal target.Each point represents an independent mouse (biological replicate) and the
382 graph shows the mean and the standard of the mean (SEM).

383

384 *Structural-based analysis of ShmB druggability*

385 The human serine hydroxymethyltransferase (SHMT) is considered a promising target for anti-cancer
386 drug development [46] and accordingly various inhibitors have been developed (see for instance [47,
387 48]). We tested the capacity of two existing inhibitors of the human SHMT, Hit-1 [49] and SHIN-1 [48],
388 to hamper *A. fumigatus* growth. However, these chemicals did not inhibit *A. fumigatus* growth at all
389 at high concentrations (30 µg/mL = 65 µM of Hit1 or 16 µg/mL =16 µM of SHIN-1), and the fungus was
390 able to grow even at very high concentrations (650 µM Hit-1 and 160 µM of SHIN-1) (Fig. S3). As our
391 previous results with the *tetOFF* promoter indicated that ShmB is essential for *A. fumigatus* viability,
392 we hypothesised that the inhibitors designed against the human enzyme may not be effective against
393 the fungal enzyme, which would imply that fungal specific inhibitors that do not have cross-toxicity

394 could also be developed. To substantiate this hypothesis our initial step involved identifying the main
395 druggable binding pocket of the human SHMT based on its crystal structure as retrieved from the
396 Protein Data Bank (accession number PDB ID 1bj4), using a target-based *in silico* approach. We
397 conducted two independent analyses employing the DrugRep [50] and the PockDrug [51] engines. The
398 PockDrug analysis yielded ten possible binding pockets, with only six of them possessing a Druggability
399 Probability score exceeding 0.5 (Fig. 5A). Cross-referencing with the results from DrugRep revealed a
400 single common pocket from both predictions: pocket A (Fig. 5A) (Gln44 Ala383 Ile51 Glu374 Phe56
401 Ser381 Ala379 Glu69 Val46 Arg43 Cys384 Ala407 Gly47 Glu49 Ile382 Arg465 Glu378 Glu54 Asn55
402 Leu48). Next, we investigated whether this predicted binding pocket is preserved in the *A. fumigatus*
403 orthologue. To this purpose, we constructed a homological model of the fungal protein using the *in*
404 *silico* protein modelling AI AlphaFold [52]. Although the similarity between the sequences is
405 reasonably high (74.9%), indicating the protein is well preserved crossed the species, there are some
406 mutations in the amino acids within the key areas associated to the hypothetical binding pocket
407 (highlighted in red in Figure 5B). A close comparison revealed that such mutations likely altered the
408 conformation of the neighbouring amino acid residues hence resulting in a different topology of
409 pocket A compared to human SHMT, making it much shallower and smaller (Figure 5C). In particular,
410 the alteration in the position of Arg263 (Arg255 in *A. fumigatus* SHMT) has formed a barrier resulting
411 in the fungal pocket being almost half the size of the human pocket A.

412 Subsequently, we performed *in silico* docking using the SwissDock engine [53, 54] employing the Hit-
413 1 inhibitor (IC50 = 0.53 µM) [49] against pocket A of the human protein. This resulted in several
414 promising binding motifs occupying the entire pocket, as visually represented in Figure 5D. For
415 instance, in one of the top binding positions, HIT1.242 (ΔG = -7.57 kcal/mol; FullFitness = -2433.57
416 kcal/mol), Hit-1 nestled itself deep into the pocket, demonstrating hydrophobic interactions with the
417 pocket (Fig. 5E). Additionally, it also formed four hydrogen bonds distributed through the molecule
418 backbone (Ser`41, Gln`44, Arg`43 and Tip3`579; Fig. 5G), anchoring the ligand neatly into the pocket
419 (Fig. 5E). Subsequent *in silico* docking between Hit-1 and the fungal orthologue pocket A suggested
420 that Hit-1 could not bind as effectively. Only two binding motifs were suggested, both restricted to
421 the smaller *A. fumigatus* pocket (Figure 5D). Upon a closer inspection of the top binding motif, HIT1.28
422 (ΔG = -6.87 kcal/mol; FullFitness = -2143.87 kcal/mol; Fig. 5G), it is clear that the ligand is not
423 embedding deep into the pocket, indicating less hydrophobic interactions with the target. There is
424 only one hydrogen bond suggested between Hit-1 and the target (ASP`55; Fig. 5F), indicating a less
425 favourable binding compared to the human version of the protein. It also appeared that the altered
426 Arg255 indeed acted as a barrier, blocking Hit-1 from extending to the region proximal to Arg43 (Arg35
427 in *A. fumigatus* SHMT) and forming any additional hydrogen bonds (Fig. 5F). Therefore, it appears that

428 Hit-1 is specific to human SHMT as it cannot bind properly to the fungal orthologue, which would agree
429 with the observed absence of growth inhibition on *A. fumigatus* (Fig. S3). Similarly, we believe that
430 inhibitors that bind to the fungal, but not the human, enzyme pocket can be designed, and thus we
431 propose that the development of novel fungal-specific inhibitor agents against the promising SmhB
432 antifungal target is feasible.

Fig. 5

A

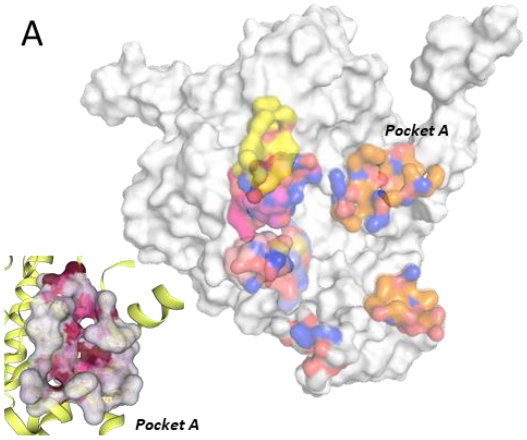

B

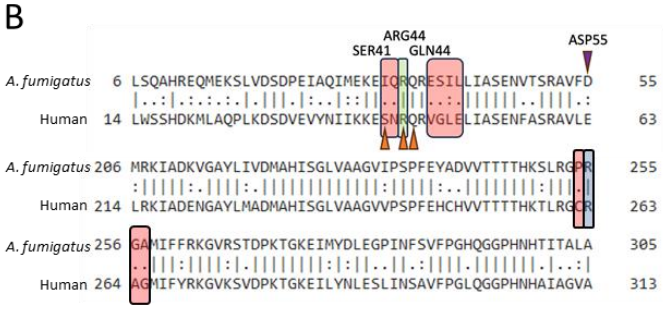

C

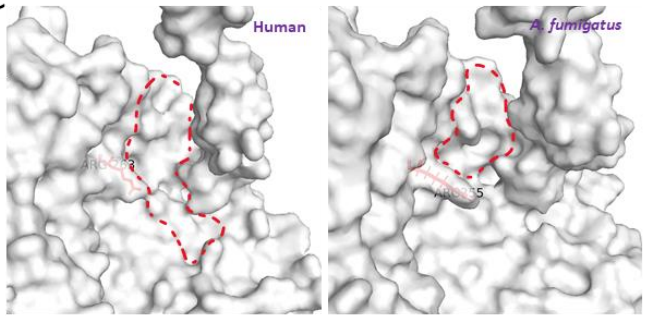

Pockets	Vol. Hull	Hydroph. Kyte	Polar Res	Aromtica Res	Drugg Prob	Standard Deviation
P1	667.66	0.18	0.47	0.20	**0.89**	**0.03**
P2	557.96	-0.03	0.50	0.06	**0.68**	**0.04**
P6	429.67	-0.03	0.42	0.08	**0.70**	**0.03**
P7	439.19	0.10	0.33	0.11	**0.79**	**0.01**
P8	407.80	-0.44	0.50	0.21	**0.69**	**0.06**
P9	473.76	0.22	0.40	0.00	**0.73**	**0.07**

D

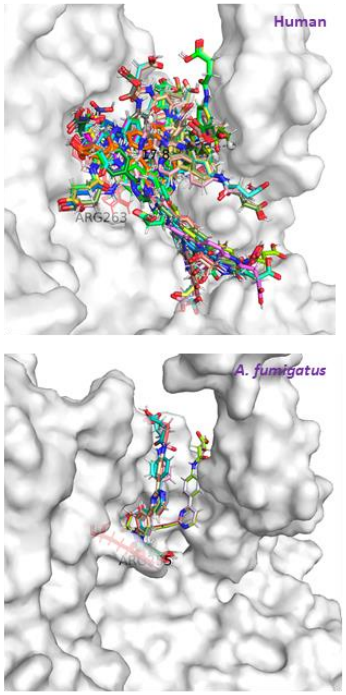

E

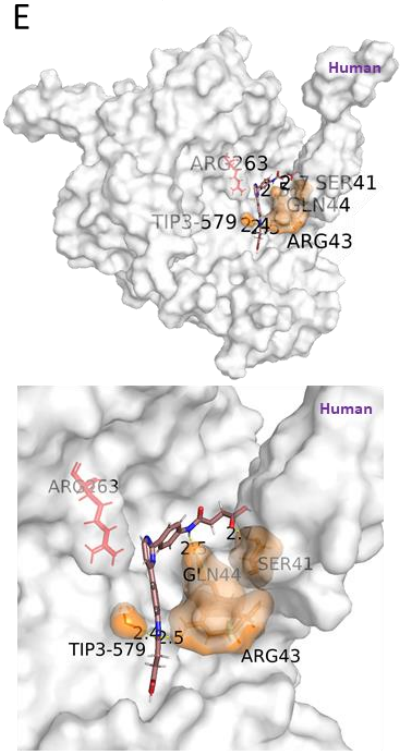

F

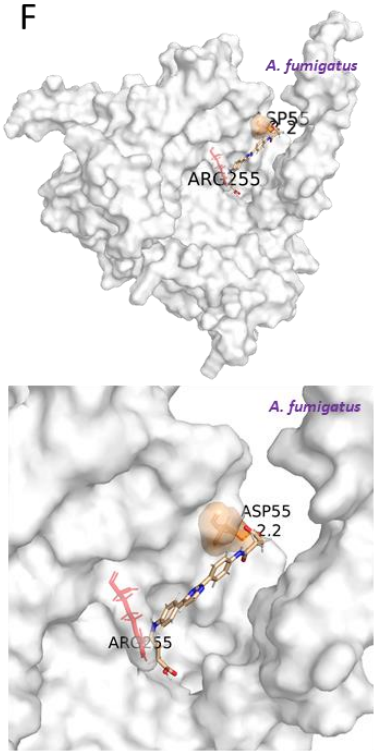

G

Hydrogen bond pairs between Hit-1 and SHMT					
Distance	2.7	2.5	2.5	2.4	2.2
Hit-1	HIT1.242/O5	HIT1.242/H16	HIT1.242/O2	HIT1.242/O2	HIT1.28/ H21
Human	SER`41/HG1	GLN`44/OE1	ARG`43/HH21	TIP3`579/H1	
A. fumigatus					ASP`55/OD1

The unit of the distance measuring is Å.

435 **Figure 5. An inhibitor of the human SHMT does not bind properly to the fungal enzyme's ligand**
436 **binding pocket**

437 **A)** Binding pockets with draggability score above 0.5 predicated by DrupRep highlighted in human
438 SHMT1 1bj4, with 'Pocket A' Zoomed in (left corner). **B)** Alignment of the amino acid sequences
439 (partial) of the *A. fumigatus* (ShmB) and human (SHMT1) cytosolic SHMT enzymes. Different amino
440 acids (highlighted in red rectangles) were detected surrounding the key residues Arg263 in SHMT1
441 (Arg255 in ShmB, highlighted in blue rectangle); and Arg43 (Arg35 in ShmB, highlighted in green
442 rectangle). Orange arrows indicate SHMT1 residues forming hydrogen bonds with Hit-1 and purple
443 arrow indicates ShmB residue forming hydrogen bond with Hit-1. **C)** Predicted binding pockets
444 comparison between SHMT1 and ShmB with Arg263 (Arg255) highlighted in red. **D)** Hit-1 binding
445 motifs suggested by SwissDock. **E)** Detailed interactions formed between Hit-1 and SHMT1. **F)** Detailed
446 interactions formed between Hit-1 and ShmB. **G)** List of hydrogen bond pairs between Hit-1 and
447 SHMT1 and ShmB.

448

449 **DISCUSION**

450 New antifungal agents are urgently needed, as resistance to the current drugs is widespread [55-57],
451 posing a great threat to human health [24]. In the endeavour of developing novel and efficient
452 chemotherapy, the selection of valid drug targets is crucial [58]. In the last few years, a variety of
453 innovative approaches have been applied to identify suitable target candidates. For instance,
454 comparative genomics [59], computer modelling [60], *in silico* analysis of protein interactions [61],
455 screening of deletion libraries [62], screening of regulatable libraries [43, 63], construction of
456 transposon insertion libraries [64, 65], or machine learning approaches [66] have been employed to
457 identify antifungal drug targets. In this regard, *in vivo* transcriptomics has also been used frequently
458 to understand fungal pathogenicity [34, 67-70], albeit its potential to identify suitable antifungal
459 targets still encounters some scepticism. In a seminal study, McDonagh and colleagues [34] compared
460 the transcriptome obtained from conidia germinating in murine lungs with germlings obtained from
461 *in vitro* conditions expected to match the *in vivo* environment. This work could confirm that *A.*
462 *fumigatus* encounters nutrient (particularly iron and nitrogen) limitation as well as alkaline and
463 oxidative stress during initiation of infection, providing foundational cues about the conditions
464 encountered by the fungal pathogen in the lungs. However, this study needed to use pools of 24 mice
465 per sample, which limited the number of conditions that could be tested (for instance, only one model
466 of immunosuppression was assayed), could only analysed the early initiation of infection (12-14 hours)
467 and had to recover the fungal material from bronchoalveolar lavages. These limitations were mainly

468 due to the challenge of recovering sufficient fungal RNA material from the infected tissue for the
469 subsequent analysis. In a more recent study, NanoString analysis was employed to identify *A.*
470 *fumigatus* transcriptional factors which are highly expressed or strongly up-regulated during growth
471 in the murine lung tissues, and experimentally proved that two of them are relevant in the context of
472 infection [71]. Here we reasoned that by comparing the transcription levels of genes related to sulfur
473 metabolism in the tissues versus a variety of *in vitro* S-sources could reveal gene products that are
474 specifically upregulated *in vivo*, and may therefore be relevant for the infection process and constitute
475 promising antifungal targets.

476 In our analysis of genes related with sulfur metabolism, we have identified 15 genes that are
477 consistently expressed at higher levels in the murine lungs than in all tested *in vitro* conditions. At
478 least 5 of those genes have been previously proven to be important for *A. fumigatus* virulence, and
479 additionally 6 genes have been suspected to be relevant as well (Table 1). We previously showed that
480 AFUA_5G02180, encoding cysteine synthase (CysB), is important for *A. fumigatus* virulence, as a
481 cysteine auxotroph had reduced virulence in a murine model of infection [14]. We have also
482 demonstrated that AFUA_8G04340 encodes cystathionine-γ-lyase (MecB), the major persulfidating
483 enzyme in *A. fumigatus*, which is relevant for fungal virulence [33]. The genes AFUA_2G07680,
484 encoding L-ornithine-*N* ^{5}-monooxygenase (SidA), which catalyses the first committed step of
485 siderophore biosynthesis, and AFUA_5G03920, encoding the master transcriptional regulator for
486 adaptation to iron limitation (HapX), have been shown to be crucial for virulence [28, 29]. Finally, the
487 gene AFUA_8G04340, encoding the transcriptional activator of the cross-pathway control system of
488 amino acid biosynthesis (CpcA), was also reported to contribute to *A. fumigatus* virulence [30].
489 Therefore, we propose that the remaining genes are also likely to be important for *A. fumigatus*
490 virulence and thus constitute good candidates to validate experimentally. It is noteworthy that genes
491 that we have characterized and shown to be dispensable for virulence (AFUA_1G05020 -*sB*- and
492 AFUA_2G15590 -*sF*- [14]) were not detected in this analysis, further supporting the hypothesis that
493 the genes identified may indeed be relevant. Nevertheless, it also needs to be mentioned that several
494 genes that have been described as relevant for virulence in other studies were not identified as
495 universally important in our analysis (for instance, AFUA_6G04700 -HisB- , AFUA_4G06530 -MetR- or
496 AFUA_2G14210 - Ilv3A/IlvC- [13, 26, 72]), implying that our approach is not able to detect all genes
497 relevant for infection. Yet, our analysis has identified some of these genes as potential disease
498 initiation or progression factors, which opens the question of whether their relevance for infection
499 might be time-dependent.

500 In fact, our temporal analysis has revealed various potential disease initiation and progression factors.
501 These are defined as products that are required for the initiation of infection or for the persistence

502 and progression of disease [35]. Differentiating these actions is paramount for drug discovery, as it
503 would not be adequate to develop a drug to treat established infections that targets an initiation
504 factor, and similarly, it would not be appropriate using a drug that targets a progressing factor as
505 prophylaxis. Therefore, discerning disease initiation and progression factors would be important to
506 better understand the infective capacity of *A. fumigatus* and to expand our reservoir of potential
507 antifungal targets. In fact, progression factors, which are usually not identified in classic virulence
508 studies, are regarded as valuable targets, as antimicrobials are often employed to treat established
509 infection [35]. In this respect, we previously negated a role of *sFα* (AFUA_6G08920) and *sB*
510 (AFUA_1G05020) in *A. fumigatus* virulence by infecting leukopenic mice with null mutants [14], but
511 our current results suggest that they might be disease progression factors specifically relevant in the
512 steroid model (Fig. 3C).

513 It was unfortunate that the samples from two leukopenic mice did not run properly and had to be
514 excluded from the analyses. We acknowledge that this limits the value of some of our results,
515 particularly the comparisons among time-points and the analysis of temporal expression of genes in
516 leukopenic mice. However, as all the infections for the *in vivo* samples of the analysis were carried out
517 simultaneously, we reasoned that repeating just two mice would not provide fully consistent results.
518 Indeed, we tried to include the data obtained from the two leukopenic mice of the preliminary
519 experiment to validate the linear amplification protocol (Fig. 1A), but found that these samples
520 clustered completely separated from all other *in vivo* samples in the study (Fig S4), and therefore could
521 not be used for the model and temporal analyses. Importantly, even if they clustered separately, the
522 overall profile of expression relative to *in vitro* remained highly similar, such that the 15 genes
523 previously detected to be consistently upregulated *in vivo* VS *in vitro* were maintained with the
524 inclusion of these mice (Fig. S4), which shows the strength of the results. In addition, with these two
525 additional mice one more gene was included in the list of candidates, AFUA_5G07210. This gene
526 encodes a homoserine O-acetyltransferase, which has been described as important for virulence in
527 the fungal pathogen *Cryptococcus neoformans* [73].

528 One of the uncharacterised genes in our list of 15 potentially relevant genes encodes a serine
529 hydroxymethyltransferase (SHMT). SHMT is a pyridoxal phosphate-dependent enzyme of the folate
530 cycle that catalyses the reversible conversion of serine and tetrahydrofolate (THF) into glycine and
531 5,10-methylenetetrahydrofolate (CH_2-THF). Fungi encode two isoforms in the nuclear genome, one
532 cytosolic and one mitochondrial [45]. In *S. cerevisiae* both genes were disrupted singly and in
533 combination, generating auxotrophic viable strains [74]. In contrast to our results, the deletant of the
534 cytosolic SHMT encoding gene (*SHM2*) grew well in the presence of the substrates glycine and
535 formate. In addition, the cytosolic and mitochondrial SHMT encoding genes could also be deleted in

536 the ascomycete *Ashbya gossypii* [75], where supplementation with adenine or glycine could
537 reconstitute growth of the cytosolic *SHMT* (*SHM2*) knock out. Therefore, essentiality of the cytosolic
538 ShmB in *A. fumigatus* suggests that the metabolic implications of disrupting the one carbon-cycle are
539 more complex in this pathogen than in other fungi. Indeed, we previously showed that in contrast to
540 other fungi, the absence of methionine synthase, which forms a junction between the one carbon
541 cycle and the trans-sulfuration pathway, causes an imbalance in cell energetics, possibly initiated by a
542 cellular sensing of purine depletion, that halts fungal growth [40]. Here we found that adenine could
543 partly reconstitute growth of the *shmB_tetOFF* strain in restrictive conditions, which resembles the
544 phenotype we observed with *metH_tetOFF* [40]; but in contrast to the absence of MetH, ATP could
545 not fully reconstitute growth in the absence of ShmB, reflecting that we do not understand the
546 metabolic implications of eliminating the cytosolic serine hydroxymethyltransferase activity. Given its
547 essentiality, we hypothesised that it could constitute a good target for the development of novel
548 antifungals, and indeed we have validated it in a murine model of established infection using the
549 *tetOFF* system. To our knowledge the relevance of serine hydroxymethyltransferases for fungal
550 pathogenicity had not been investigated before. In contrast, this enzyme has been shown to be a
551 promising antimalarial target [76] and implicated in a variety of virulence related traits in bacteria. For
552 instance, a null mutant in *Staphylococcus aureus* showed impaired survival inside macrophages and
553 reduced virulence in a *Galleria mellonella* infection model [77]. In *Helicobacter pylori*, deletion of the
554 SHMT encoding gene *glyA* caused reduced growth rate [78], and in *Pseudomonas aeruginosa* controls
555 rugose colony morphology, increases biofilm formation, abolishes swarming and relates to the redox
556 status of the cells and the control of iron acquisition [79]. Therefore, targeting microbial SMHT
557 enzymes seems to be a promising antimicrobial strategy. Nevertheless, as the current SHMT inhibitors
558 have been developed against the human enzyme, specific inhibitors against the microbial proteins
559 need to be designed. By comparing the pocket landscape of the *A. fumigatus* and human enzymes and
560 performing a docking assay with a known inhibitor of the human SHMT, here we show that there are
561 sufficient differences to pursue the development of a fungal specific agent. A comparable situation
562 occurs in the case of efforts to inhibit the promising antifungal target calcineurin. The human and
563 fungal enzymes are highly similar, such that a drug developed against the human protein, FK506, also
564 inhibits the fungal enzyme and it is a potent antifungal agent. Current research aims to develop FK506
565 derivatives that are fungal specific, and much of this work is fuelled by structural insight [80-82].

566 In conclusion, in this study we show that *in vivo* transcriptomics is a valid strategy to identify virulence
567 traits in *A. fumigatus*. Using the NanoString technology we have detected 15 genes as potentially
568 relevant for pathogenicity, five of which have already been proven experimentally. We further
569 investigate one novel gene, encoding the cytosolic serine hydroxymethyltransferase, thereby

570 demonstrating that this is an essential gene product in *A. fumigatus* and that it seems possible to
571 specifically inhibit the enzyme's activity. Therefore, we have validated cSHMT as a promising
572 antifungal target for future research efforts.

573

574 **MATERIAL AND METHODS**

575 *Fungal strains and culture media*

576 The *Aspergillus fumigatus* strain ATCC46645 [83] was used for the transcriptomic analysis, and the
577 MFIG001 isolate (*ΔKU80*) for genetic manipulation [84]. The strains were routinely grown on
578 Sabouraud solid medium (Oxoid) for 3-5 days at 37 °C for spore harvesting.

579 For phenotyping analysis, the isolates were inoculated on solid *Aspergillus* Minimal Medium (AMM,
580 1% glucose, 5 mM ammonium tartrate, 7 mM KCl, 11 mM KH_2PO_4, 0.25 mM $MgSO_4$, 1× Hutner's trace
581 elements solution [pH 5.5], 1.5% agar), supplemented as indicated in each section, and incubated at
582 37 °C for 2-3 days. Phenotypic experiments were performed at least twice independently.

583 For selection in the presence of resistance markers 50 µg ml^{-1} of hygromycin B or 100 µg ml^{-1} of
584 pyrithiamine (InvivoGen) were added to the AMM in the growth plates.

585

586 *Mutant construction*

587 To generate the *ΔshmA* mutant and attempt to construct the *ΔshmB* mutant, we followed a previously
588 optimised protocol [85]. Briefly, upstream and downstream fragments of the genes were amplified by
589 HIFI-PCR and fused to the Hygromycin-B (*hph*) selective cassette by fusion PCR. This deletant cassette
590 was used to replace the target gene by homologous recombination in the *ΔKU80* strain MFIG001.

591 To construct the *shmB_tetOFF* isolate, we followed CRISPR-Cas9 mediated recombination, as
592 previously described for *A. fumigatus* [86]. Briefly, a repair template containing the *tetOFF* module
593 and a pyrithiamine resistance marker (PtrA), was amplified from pSK606 [39] using Phusion green hot
594 start II high-fidelity PCR master mix (ThermoFisher Scientific). The repair template had 50 bp flanking
595 regions homologous to the upstream and downstream sequences at the ATG start codon, placing the
596 *tetOFF* module immediately 5'- of the *shmB* ORF. The sequence of the targeted gRNA (crRNA) was
597 (GTCCAAATGAAAGAAAACAA|TGG) and was designed using EuPaGDT [87].

598 To construct the fluorescent SHMT strains, we inserted the correspondent repair template, containing
599 Citrine and the pyrithiamine resistance marker, at the 3'-UTR of each gene using CRISPR-Cas9 as

600 previously descried [86]. Each repair template carried flanking homology regions to the targeted gene.
601 The targeted gRNAs used were (5'-GACAGGCAGGGGGTAGGTGC-3') and (5'-
602 GGGCACTTTCAGCCTTCCGT-3') for *shmB* and *shmA*, respectively.

603 All primers used in the study can be found in Table S3.

604

605 *Localisation studies of ShmB-Citrine*

606 *A. fumigatus* conidia were inoculated in 200 µL of filtered autoclaved AMM on 8 well chambers slides
607 (IBIDI) and incubated at 30 °C for 16h. Imagining was performed using a Leica SP8x laser scanning
608 confocal microscope equipped with a 63x (NA 1.4) HC PLAN APO CS2 oil immersion objective. The
609 pinhole was set to one Airy unit and the gain was set to 200. To visualise the localisation of labelled
610 proteins, fluorescence imaging was performed using an excitation of 516 nm and 529 nm emission
611 using a white light laser. Image format captures was 1024x1024 at 400 hz scan speed. Z-stacks of
612 germlings were taken at 1.0 microns and slices were projected as average intensity using ImageJ no
613 adjustments to brightness or contrast were made. Scale bars are shown.

614

615 *Murine Infections*

616 Mouse infections experiments were performed under United Kingdom Home Office project license
617 PDF8402B7 and approved by the University of Manchester Ethics Committee and by the Biological
618 Services Facility at the Faculty of Biology, Medicine and Health, University of Manchester.

619 Outbred CD1 male mice (22 to 26 g) were purchased from Charles Rivers and left to rest for at least
620 one week before the experiment. Mice were allowed access *ad libitum* to water and food throughout
621 the experiment.

622 For the leukopenic model mice were immunosuppressed with 150 mg/kg of cyclophosphamide
623 (Baxter) on days −3 and −1 plus 1 subcutaneous injection of 250 mg/kg hydrocortisone 21-Acetate
624 (Sigma-Aldrich) on day −1. For the corticosteroid model, mice were injected with a single dose of 40
625 mg/kg of triamcinolone (Bristol Myers Squibb) on day −1. Bacterial infections were prevented by
626 adding 2 g/L neomycin to the drinking water. Mice were anesthetized by exposure to 2% to 3%
627 isoflurane (Sigma-Aldrich) for 5 to 10 minutes and intranasally infected with 40 µL of a suspension
628 containing 10^5 spores for the leukopenic model and 10^6 spores for the corticosteroid model. For both
629 models, 3 mice per time point post infection (16, 24 or 72h) were used. At the designated time-points,

630 mice were sacrificed by a lethal injection of pentobarbital and the lungs were harvested to be
631 immediately snap frozen for RNA isolation.

632 For the chronic model, we followed a published protocol [25, 88]. Briefly, an immunocompetent
633 mouse was anesthetised by intraperitoneal injection of a ketamine (1%)/xylazine (0,2%) solution and
634 intratracheally inoculated with 50 µL of a suspension of agar beads containing 5×10^7 conidia/mL.
635 Infection was left to progress for 21 days before the mouse was sacrificed for further processing.

636 To monitor virulence of the *shmB_tetOFF* strain, we followed our previously optimised protocol [40].
637 Briefly, groups of 10 mice were infected with 40 µL of a suspension containing 2×10^5 of the
638 *shmB_tetOFF* or the control *Δcyp51B-cyp51A-tetOFF* strain (inocula were confirmed by plating
639 dilutions of the used suspensions). Five mice per strain received doxycycline (Dox) treatment and five
640 PBS vehicle. Dox treatment started 16h after infection by an intraperitoneal injection (50 mg/kg) and
641 change to Dox-containing food (Envingo Safe-Diet U8200 version 0115 A03 0.625 g/kg Doxycycline
642 Hyclate pellets). Treatment was maintained by subcutaneous 50 mg/kg Dox injections every 12h post
643 infection until the end of the experiment after 72h.

644

645 *NanoString analysis: Preparation of samples, hybridisation and data processing*

646 RNA from *in vitro* conditions was isolated as previously described [13]. Briefly, mycelia were shifted
647 from a culture grown overnight in AMM to new flasks containing the defined sources described in
648 Table S2. Mycelia were incubated for 4h in the new conditions, then filtrated trough sterile Miracloth
649 (Merck Millipore) and snap frozen in liquid nitrogen. Mycelia were ground in the constant presence of
650 liquid nitrogen and RNA was isolated using the RNeasy Plant Mini Kit (Qiagen) following the
651 manufacturer's instructions and including the on column DNAse digestion step. RNA was assessed by
652 a NanoDrop 2000 spectrophotometer (Thermo Fisher Scientific) to determine quality and
653 concentration.

654 RNA from murine lungs was isolated as follows: Lungs were lyophilized for 48h in a CoolSafe ScanVac
655 freeze drier connected to a VacuuBrand pump and subsequently ground in the presence of liquid
656 nitrogen. The resulting powder was resuspended in TRIzol reagent (Invitrogen – Thermofisher) and
657 processed following the manufacturer's instructions. RNA was cleaned with
658 Phenol:Chloroform:Isoamyl (25:24:1) (Sigma) and extracted with Chloroform (Invitrogen).
659 Subsequently, RNA was purified using the RNeasy Minikit (Qiagen), following the clean-up protocol,
660 and including the on column DNAse digestion step.

661 RNA isolated from murine lungs was subjected to the NanoString nCounter Single Cell Gene Expression
662 protocol for linear amplification of target genes. Briefly, RNA was converted to cDNA using SuperScript
663 VILO MasterMix (Life Technologies). To confirm that target RNA was present in the samples, and that
664 cDNA has been properly generated, a Real-Time PCR was performed using the gene AFUA_4G07360
665 (*metH*) as target, as a RT-PCR for this transcript had been validated before [40]. Genes of interest were
666 linearly amplified using the Multiplex Target Enrichment (MTE) primers (Supplementary File 1) and a
667 PCR protocol consisting of 16 MTE amplification cycles of 94°C 15 seconds and 60°C 4 minutes, with
668 the TaqMan PreAmp Master Mix (Life Technologies).

669 cDNA samples were incubated for 2 minutes at 94°C and then snap cool on ice prior to addition to the
670 hybridization reaction. Hybridization was performed according to the Elements Tagset Hybridisation
671 setup, as detailed by Nanostring and using the NanoString custom designed probes A and B
672 (Supplementary File 1). The cartridge was read using the flex system, consisting of nCounter Prep
673 Station and the Digital Analyser.

674 The saw data file (Supplementary File S2) was initially subjected to a Quality Control check. This
675 consisted of the monitorization of the counts of the internal positive control (positive performance
676 for hybridization verification) and the total counts detected for each of the conditions (Fig. S1).

677 Raw data (Supplementary File 2) was normalised using the nSolver 4.0 software (NanoString). Data
678 was first subjected to Background Subtraction using the geometric mean of the negative control
679 counts. Subsequently, data was normalized using both the geometric mean of positive control count
680 and the geometric mean of the housekeeping genes (Supplementary File 3).

681 Normalised data was analysed using the Agglomerative Cluster – Heat map option of the nSolver 4.0
682 software (NanoString). Spearman Correlation was used as distance metric and Average was used as
683 linkage method.

684

685 *Computational structure analyses*

686 The crystal structure of the serine hydroxymethyltransferase (SHMT) was obtained from Research
687 Collaboratory for Structural Bioinformatics Protein Data Bank (RCSB PDB, http://www.rcsb.org) in PDB
688 format, referenced by its protein data bank ID 1bj4. The structure of the fungal SHMT was predicted
689 using AlphaFold2 [52]. The amino acid sequence was retrieved from FungiDatabase [89] and utilised
690 as input, with the highest scoring model (pLDDT= 96.9, pTMscore= 0.943) selected for downstream *in*
691 *silico* analysis.

692 For the human SHMT, DrugRep [50] and PockDrug [51] were employed for target based binding pocket
693 prediction. DrugRep is a receptor-based screening tool utilising CB-Dock to identify docking pockets
694 of the protein receptor. PockDrug utilizes the fpocket estimation method, based on holo or apo
695 proteins, for predicted pocket estimation. This method involves preliminary detection of cavities
696 capable of binding a ligand of sufficient size, though without ligand proximity information. Pockets
697 with a predicted druggability score above 0.5 from DrugRep were recorded and cross-referenced with
698 suggestions from PockDoc to determine the 'optimal' binding pocket for subsequent *in-silico* docking.

699 Ligand Hit-1 was drawn using Marvin JS (https://marvinjs-demo.chemaxon.com/latest/demo.html
700 [90]). The binding mode of Hit-1 to optimal binding pocket in SHMT was predicted using the EADock
701 DS based SwissDock (http://www.swissdock.ch/docking# [54]). The binding modes with the most
702 favourable energies were evaluated with FACTS (Fast Analytical Continuum Treatment of Solvation
703 [91]) and then output as clusters. The best docking pose, exhibiting maximal hydrophobicity pockets
704 coverage and hydrogen bonding, was manually selected. Outputs from all programmes were
705 visualised in PyMOL 2.5 (Schrödinger, LLC).

706

707

708 **ACKOWLEDGEMENTS**

709 We would like to specially thank Prof Sven Krappmann, who guided JA to discover the NanoString
710 technology some years ago and so inspired this work. In addition, we would like to thank Emilia
711 Mellado and Sven Krappmann for critical reading of the manuscript. We acknowledge the use of the
712 Genomic Technologies Facility (Faculty of Biology Medicine and Health, University of Manchester) for
713 the NanoString hybridisation and data read. Help and support from members of the Manchester
714 Fungal Infection Group (MFIG) and the Spanish National Centre for Mycology (LRIM) is greatly
715 appreciated.

716 This work was funded by the MRC Career Development Award (MR/N008707/1)

717 **REFERENCES**

718 1. Tekaia, F. and J.P. Latge, *Aspergillus fumigatus: saprophyte or pathogen?* Curr Opin Microbiol,
719 2005. **8**(4): p. 385-92.
720 2. Hospenthal, D.R., K.J. Kwon-Chung, and J.E. Bennett, *Concentrations of airborne Aspergillus*
721 *compared to the incidence of invasive aspergillosis: lack of correlation.* Med Mycol, 1998.
722 **36**(3): p. 165-8.
723 3. Latge, J.P., *Aspergillus fumigatus and aspergillosis.* Clin Microbiol Rev, 1999. **12**(2): p. 310-50.
724 4. Park, S.J. and B. Mehrad, *Innate Immunity to Aspergillus Species.* Clinical Microbiology
725 Reviews, 2009. **22**(4): p. 535-551 DOI: 10.1128/cmr.00014-09.
726 5. Kosmidis, C. and D.W. Denning, *The clinical spectrum of pulmonary aspergillosis.* Thorax, 2015.
727 **70**(3): p. 270-7 DOI: 10.1136/thoraxjnl-2014-206291.
728 6. Lowes, D., et al., *Predictors of mortality in chronic pulmonary aspergillosis.* Eur Respir J, 2017.
729 **49**(2) DOI: 10.1183/13993003.01062-2016.
730 7. Brown, G.D., et al., *Hidden killers: human fungal infections.* Sci Transl Med, 2012. **4**(165): p.
731 165rv13 DOI: 10.1126/scitranslmed.3004404.
732 8. Lestrade, P.P., et al., *Voriconazole Resistance and Mortality in Invasive Aspergillosis: A*
733 *Multicenter Retrospective Cohort Study.* Clin Infect Dis, 2019. **68**(9): p. 1463-1471 DOI:
734 10.1093/cid/ciy859.
735 9. Meis, J.F., et al., *Clinical implications of globally emerging azole resistance in Aspergillus*
736 *fumigatus.* Philos Trans R Soc Lond B Biol Sci, 2016. **371**(1709) DOI: 10.1098/rstb.2015.0460.
737 10. Scott, J. and J. Amich, *Primary Metabolism of Human Pathogenic Fungi, Importance for*
738 *Virulence and Potential for Drug Development*, in *Encyclopedia of Infection and Immunity*.
739 2022. p. 377-407.
740 11. Ene, I.V., et al., *Metabolism in Fungal Pathogenesis.* Cold Spring Harbor Perspectives in
741 Medicine, 2014. **4**(12): p. a019695-a019695 DOI: 10.1101/cshperspect.a019695.
742 12. Amich, J., S. Krappmann, and A.K. Bachhawat, *Editorial: Sulphur Metabolism of Fungi -*
743 *Implications for Virulence and Opportunities for Therapy.* Frontiers in Microbiology, 2020. **11**
744 DOI: 10.3389/fmicb.2020.583689.
745 13. Amich, J., et al., *Regulation of sulphur assimilation is essential for virulence and affects iron*
746 *homeostasis of the human-pathogenic mould Aspergillus fumigatus.* PLoS Pathog, 2013. **9**(8):
747 p. e1003573 DOI: 10.1371/journal.ppat.1003573.
748 14. Amich, J., et al., *Exploration of Sulfur Assimilation of Aspergillus fumigatus Reveals*
749 *Biosynthesis of Sulfur-Containing Amino Acids as a Virulence Determinant.* Infect Immun,
750 2016. **84**(4): p. 917-29 DOI: 10.1128/IAI.01124-15.
751 15. Scott, J., et al., *Targeting Methionine Synthase in a Fungal Pathogen Causes a Metabolic*
752 *Imbalance That Impacts Cell Energetics, Growth, and Virulence.* mBio, 2020. **11**(5) DOI:
753 10.1128/mBio.01985-20.
754 16. Traynor, A.M., et al., *Involvement of Sulfur in the Biosynthesis of Essential Metabolites in*
755 *Pathogenic Fungi of Animals, Particularly Aspergillus spp.: Molecular and Therapeutic*
756 *Implications.* Frontiers in Microbiology, 2019. **10** DOI: 10.3389/fmicb.2019.02859.
757 17. Bachhawat, A.K. and A.K. Yadav, *Metabolic Pathways as Drug Targets: Targeting the Sulphur*
758 *Assimilatory Pathways of Yeast and Fungi for Novel Drug Discovery*, in *Combating Fungal*
759 *Infections*. 2010. p. 327-346.
760 18. Kuplińska, A. and K. Rząd, *Molecular targets for antifungals in amino acid and protein*
761 *biosynthetic pathways.* Amino Acids, 2021. **53**(7): p. 961-991 DOI: 10.1007/s00726-021-
762 03007-6.
763 19. Xu, W., et al., *Pathogen Gene Expression Profiling During Infection Using a Nanostring*
764 *nCounter Platform*, in *Yeast Functional Genomics*. 2016. p. 57-65.

20. Bourré, L., *Genome-Wide RNAseq and Array-Based NanoString Transcriptomic Technologies: Which To Use and When? - Crown Bioscience*. 2020: https://blog.crownbio.com/genome-wide-rnaseq-and-array-based-nanostring-transcriptomic-technologies.
21. Veldman-Jones, M.H., et al., *Evaluating Robustness and Sensitivity of the NanoString Technologies nCounter Platform to Enable Multiplexed Gene Expression Analysis of Clinical Samples.* Cancer Research, 2015. **75**(13): p. 2587-2593 DOI: 10.1158/0008-5472.Can-15-0262.
22. Geiss, G.K., et al., *Direct multiplexed measurement of gene expression with color-coded probe pairs.* Nature Biotechnology, 2008. **26**(3): p. 317-325 DOI: 10.1038/nbt1385.
23. Fisher, M.C., et al., *Tackling the emerging threat of antifungal resistance to human health.* Nature Reviews Microbiology, 2022. **20**(9): p. 557-571 DOI: 10.1038/s41579-022-00720-1.
24. Fisher, M.C., et al., *Worldwide emergence of resistance to antifungal drugs challenges human health and food security.* Science, 2018. **360**(6390): p. 739-742 DOI: 10.1126/science.aap7999.
25. Urb, M., et al., *Evolution of the Immune Response to Chronic Airway Colonization with Aspergillus fumigatus Hyphae.* Infection and Immunity, 2015. **83**(9): p. 3590-3600 DOI: 10.1128/iai.00359-15.
26. Dietl, A.-M., et al., *Histidine biosynthesis plays a crucial role in metal homeostasis and virulence of Aspergillus fumigatus.* Virulence, 2016. **7**(4): p. 465-476 DOI: 10.1080/21505594.2016.1146848.
27. Wangsanut, T. and M. Pongpom, *The Role of the Glutathione System in Stress Adaptation, Morphogenesis and Virulence of Pathogenic Fungi.* International Journal of Molecular Sciences, 2022. **23**(18) DOI: 10.3390/ijms231810645.
28. Schrettl, M., et al., *HapX-mediated adaption to iron starvation is crucial for virulence of Aspergillus fumigatus.* PLoS Pathog, 2010. **6**(9): p. e1001124.
29. Schrettl, M., et al., *Siderophore biosynthesis but not reductive iron assimilation is essential for Aspergillus fumigatus virulence.* J Exp Med, 2004. **200**(9): p. 1213-9.
30. Krappmann, S., et al., *The Aspergillus fumigatus transcriptional activator CpcA contributes significantly to the virulence of this fungal pathogen.* Mol Microbiol, 2004. **52**(3): p. 785-99.
31. Liu, T.-B. and C. Xue, *The Ubiquitin-Proteasome System and F-box Proteins in Pathogenic Fungi.* Mycobiology, 2018. **39**(4): p. 243-248 DOI: 10.5941/myco.2011.39.4.243.
32. Jöhnk, B., et al., *SCF Ubiquitin Ligase F-box Protein Fbx15 Controls Nuclear Co-repressor Localization, Stress Response and Virulence of the Human Pathogen Aspergillus fumigatus.* PLOS Pathogens, 2016. **12**(9) DOI: 10.1371/journal.ppat.1005899.
33. Sueiro-Olivares, M., et al., *Fungal and host protein persulfidation are functionally correlated and modulate both virulence and antifungal response.* PLOS Biology, 2021. **19**(6) DOI: 10.1371/journal.pbio.3001247.
34. McDonagh, A., et al., *Sub-telomere directed gene expression during initiation of invasive aspergillosis.* PLoS Pathog, 2008. **4**(9): p. e1000154 DOI: 10.1371/journal.ppat.1000154.
35. Cramer, R.A. and C.H. Kowalski, *Is It Time To Kill the Survival Curve? A Case for Disease Progression Factors in Microbial Pathogenesis and Host Defense Research.* mBio, 2021. **12**(1) DOI: 10.1128/mBio.03483-20.
36. Savojardo, C., et al., *DeepMito: accurate prediction of protein sub-mitochondrial localization using convolutional neural networks.* Bioinformatics, 2020. **36**(1): p. 56-64 DOI: 10.1093/bioinformatics/btz512.
37. Hawkins, J. and M. BodÉN, *Detecting and Sorting Targeting Peptides with Neural Networks and Support Vector Machines.* Journal of Bioinformatics and Computational Biology, 2011. **04**(01): p. 1-18 DOI: 10.1142/s0219720006001771.
38. Almagro Armenteros, J.J., et al., *Detecting sequence signals in targeting peptides using deep learning.* Life Science Alliance, 2019. **2**(5) DOI: 10.26508/lsa.201900429.
39. Wanka, F., et al., *Tet-on, or Tet-off, that is the question: Advanced conditional gene expression in Aspergillus.* Fungal Genet Biol, 2016. **89**: p. 72-83 DOI: 10.1016/j.fgb.2015.11.003.

40. Scott, J., et al., *Targeting Methionine Synthase in a Fungal Pathogen Causes a Metabolic Imbalance That Impacts Cell Energetics, Growth, and Virulence.* mBio, 2020. **11**(5) DOI: 10.1128/mBio.01985-20.
41. Beattie, S.R., et al., *Filamentous fungal carbon catabolite repression supports metabolic plasticity and stress responses essential for disease progression.* PLoS Pathog, 2017. **13**(4): p. e1006340 DOI: 10.1371/journal.ppat.1006340.
42. Cramer, R.A., *In vivo veritas: Aspergillus fumigatus proliferation and pathogenesis--conditionally speaking.* Virulence, 2016. **7**(1): p. 7-10 DOI: 10.1080/21505594.2015.1134074.
43. Hu, W., et al., *Essential Gene Identification and Drug Target Prioritization in Aspergillus fumigatus.* PLoS Pathogens, 2007. **3**(3) DOI: 10.1371/journal.ppat.0030024.
44. Scott, J., et al., *Pseudomonas aeruginosa-Derived Volatile Sulfur Compounds Promote Distal Aspergillus fumigatus Growth and a Synergistic Pathogen-Pathogen Interaction That Increases Pathogenicity in Co-infection.* Front Microbiol, 2019. **10**: p. 2311 DOI: 10.3389/fmicb.2019.02311.
45. Cossins, E.A. and L. Chen, *Folates and one-carbon metabolism in plants and fungi.* Phytochemistry, 1997. **45**(3): p. 437-452 DOI: 10.1016/s0031-9422(96)00833-3.
46. Scaletti, E., et al., *Structural basis of inhibition of the human serine hydroxymethyltransferase SHMT2 by antifolate drugs.* FEBS Letters, 2019. **593**(14): p. 1863-1873 DOI: 10.1002/1873-3468.13455.
47. Geeraerts, S.L., et al., *The ins and outs of serine and glycine metabolism in cancer.* Nature Metabolism, 2021. **3**(2): p. 131-141 DOI: 10.1038/s42255-020-00329-9.
48. Ducker, G.S., et al., *Human SHMT inhibitors reveal defective glycine import as a targetable metabolic vulnerability of diffuse large B-cell lymphoma.* Proceedings of the National Academy of Sciences, 2017. **114**(43): p. 11404-11409 DOI: 10.1073/pnas.1706617114.
49. Nonaka, H., et al., *Design strategy for serine hydroxymethyltransferase probes based on retro-aldol-type reaction.* Nature Communications, 2019. **10**(1) DOI: 10.1038/s41467-019-08833-7.
50. Gan, J.-h., et al., *DrugRep: an automatic virtual screening server for drug repurposing.* Acta Pharmacologica Sinica, 2022. **44**(4): p. 888-896 DOI: 10.1038/s41401-022-00996-2.
51. Hussein, H.A., et al., *PockDrug-Server: a new web server for predicting pocket druggability on holo and apo proteins.* Nucleic Acids Research, 2015. **43**(W1): p. W436-W442 DOI: 10.1093/nar/gkv462.
52. Jumper, J., et al., *Highly accurate protein structure prediction with AlphaFold.* Nature, 2021. **596**(7873): p. 583-589 DOI: 10.1038/s41586-021-03819-2.
53. Grosdidier, A., V. Zoete, and O. Michielin, *Fast docking using the CHARMM force field with EADock DSS.* J Comput Chem, 2011. **32**(10): p. 2149-59 DOI: 10.1002/jcc.21797.
54. Grosdidier, A., V. Zoete, and O. Michielin, *SwissDock, a protein-small molecule docking web service based on EADock DSS.* Nucleic Acids Res, 2011. **39**(Web Server issue): p. W270-7 DOI: 10.1093/nar/gkr366.
55. Lestrade, P.P.A., et al., *Triazole resistance in Aspergillus fumigatus: recent insights and challenges for patient management.* Clinical Microbiology and Infection, 2019. **25**(7): p. 799-806 DOI: 10.1016/j.cmi.2018.11.027.
56. Pristov, K.E. and M.A. Ghannoum, *Resistance of Candida to azoles and echinocandins worldwide.* Clinical Microbiology and Infection, 2019. **25**(7): p. 792-798 DOI: 10.1016/j.cmi.2019.03.028.
57. Zafar, H., et al., *A titanic drug resistance threat in Cryptococcus neoformans.* Current Opinion in Microbiology, 2019. **52**: p. 158-164 DOI: 10.1016/j.mib.2019.11.001.
58. Mota Fernandes, C., et al., *The Future of Antifungal Drug Therapy: Novel Compounds and Targets.* Antimicrobial Agents and Chemotherapy, 2021. **65**(2) DOI: 10.1128/aac.01719-20.
59. Abadio, A.K.R., et al., *Comparative genomics allowed the identification of drug targets against human fungal pathogens.* BMC Genomics, 2011. **12**(1) DOI: 10.1186/1471-2164-12-75.

60. Bencurova, E., et al., *Identification of Antifungal Targets Based on Computer Modeling.* Journal of Fungi, 2018. **4**(3) DOI: 10.3390/jof4030081.
61. Chaudhary, R., et al., *In Silico Protein Interaction Network Analysis of Virulence Proteins Associated with Invasive Aspergillosis for Drug Discovery.* Current Topics in Medicinal Chemistry, 2019. **19**(2): p. 146-155 DOI: 10.2174/1568026619666181120150633.
62. Noble, S.M., et al., *Systematic screens of a Candida albicans homozygous deletion library decouple morphogenetic switching and pathogenicity.* Nature Genetics, 2010. **42**(7): p. 590-598 DOI: 10.1038/ng.605.
63. Becker, J.M., et al., *Pathway analysis of Candida albicans survival and virulence determinants in a murine infection model.* Proceedings of the National Academy of Sciences, 2010. **107**(51): p. 22044-22049 DOI: 10.1073/pnas.1009845107.
64. Ianiri, G., et al., *Essential Gene Discovery in the Basidiomycete Cryptococcus neoformans for Antifungal Drug Target Prioritization.* mBio, 2015. **6**(2) DOI: 10.1128/mBio.02334-14.
65. Segal, E.S., et al., *Gene Essentiality Analyzed by In Vivo Transposon Mutagenesis and Machine Learning in a Stable Haploid Isolate of Candida albicans.* MBio, 2018. **9**(5) DOI: 10.1128/mBio.02048-18.
66. Fu, C., et al., *Leveraging machine learning essentiality predictions and chemogenomic interactions to identify antifungal targets.* Nature Communications, 2021. **12**(1) DOI: 10.1038/s41467-021-26850-3.
67. Chung, D., et al., *ChIP-seq and In Vivo Transcriptome Analyses of the Aspergillus fumigatus SREBP SrbA Reveals a New Regulator of the Fungal Hypoxia Response and Virulence.* PLoS Pathogens, 2014. **10**(11) DOI: 10.1371/journal.ppat.1004487.
68. Cheng, S., et al., *Profiling of Candida albicans Gene Expression During Intra-abdominal Candidiasis Identifies Biologic Processes Involved in Pathogenesis.* The Journal of Infectious Diseases, 2013. **208**(9): p. 1529-1537 DOI: 10.1093/infdis/jit335.
69. Xu, W., et al., *Activation and Alliance of Regulatory Pathways in C. albicans during Mammalian Infection.* PLOS Biology, 2015. **13**(2) DOI: 10.1371/journal.pbio.1002076.
70. Amorim-Vaz, S., et al., *RNA Enrichment Method for Quantitative Transcriptional Analysis of Pathogens In Vivo Applied to the Fungus Candida albicans.* mBio, 2015. **6**(5) DOI: 10.1128/mBio.00942-15.
71. Liu, H., et al., *Determining Aspergillus fumigatus transcription factor expression and function during invasion of the mammalian lung.* PLOS Pathogens, 2021. **17**(3) DOI: 10.1371/journal.ppat.1009235.
72. Nielsen, K., et al., *The Aspergillus fumigatus Dihydroxyacid Dehydratase Ilv3A/IlvC Is Required for Full Virulence.* PLoS ONE, 2012. **7**(9) DOI: 10.1371/journal.pone.0043559.
73. Nazi, I., et al., *Role of homoserine transacetylase as a new target for antifungal agents.* Antimicrobial Agents and Chemotherapy, 2007. **51**(5): p. 1731-1736 DOI: 10.1128/Aac.01400-06.
74. Kastanos, E.K., Y.Y. Woldman, and D.R. Appling, *Role of Mitochondrial and Cytoplasmic Serine Hydroxymethyltransferase Isozymes in de Novo Purine Synthesis in Saccharomyces cerevisiae.* Biochemistry, 1997. **36**(48): p. 14956-14964 DOI: 10.1021/bi971610n.
75. Schlüpen, C., et al., *Disruption of the SHM2 gene, encoding one of two serine hydroxymethyltransferase isoenzymes, reduces the flux from glycine to serine in Ashbya gossypii.* Biochemical Journal, 2003. **369**(2): p. 263-273 DOI: 10.1042/bj20021224.
76. Schwertz, G., et al., *Antimalarial Inhibitors Targeting Serine Hydroxymethyltransferase (SHMT) with in Vivo Efficacy and Analysis of their Binding Mode Based on X-ray Cocrystal Structures.* Journal of Medicinal Chemistry, 2017. **60**(12): p. 4840-4860 DOI: 10.1021/acs.jmedchem.7b00008.
77. Batool, N., et al., *Functional Identification of Serine Hydroxymethyltransferase as a Key Gene Involved in Lysostaphin Resistance and Virulence Potential of Staphylococcus aureus Strains.* International Journal of Molecular Sciences, 2020. **21**(23) DOI: 10.3390/ijms21239135.

78. Antunes, L.C.M., et al., *Structural and functional insight into serine hydroxymethyltransferase from Helicobacter pylori.* Plos One, 2018. **13**(12) DOI: 10.1371/journal.pone.0208850.
79. Pu, M., et al., *Serine Hydroxymethyltransferase ShrA (PA2444) Controls Rugose Small-Colony Variant Formation in Pseudomonas aeruginosa.* Frontiers in Microbiology, 2018. **9** DOI: 10.3389/fmicb.2018.00315.
80. Juvvadi, P.R., et al., *Harnessing calcineurin-FK506-FKBP12 crystal structures from invasive fungal pathogens to develop antifungal agents.* Nature Communications, 2019. **10**(1) DOI: 10.1038/s41467-019-12199-1.
81. Gobeil, S.M.C., et al., *Leveraging Fungal and Human Calcineurin-Inhibitor Structures, Biophysical Data, and Dynamics To Design Selective and Nonimmunosuppressive FK506 Analogs.* mBio, 2021. **12**(6) DOI: 10.1128/mBio.03000-21.
82. Lee, Y., et al., *In Vitro and In Vivo Assessment of FK506 Analogs as Novel Antifungal Drug Candidates.* Antimicrobial Agents and Chemotherapy, 2018. **62**(11) DOI: 10.1128/aac.01627-18.
83. Hearn, V.M. and D.W. Mackenzie, *Mycelial antigens from two strains of Aspergillus fumigatus: an analysis by two-dimensional immunoelectrophoresis.* Mykosen, 1980. **23**(10): p. 549-62.
84. Bertuzzi, M., et al., *On the lineage of Aspergillus fumigatus isolates in common laboratory use.* Medical Mycology, 2021. **59**(1): p. 7-13 DOI: 10.1093/mmy/myaa075.
85. Zhao, C., et al., *High-Throughput Gene Replacement in Aspergillus fumigatus.* Current Protocols in Microbiology, 2019. **54**(1) DOI: 10.1002/cpmc.88.
86. van Rhijn, N., et al., *Development of a marker-free mutagenesis system using CRISPR-Cas9 in the pathogenic mould Aspergillus fumigatus.* Fungal Genetics and Biology, 2020. **145** DOI: 10.1016/j.fgb.2020.103479.
87. Peng, D. and R. Tarleton, *EuPaGDT: a web tool tailored to design CRISPR guide RNAs for eukaryotic pathogens.* Microbial Genomics, 2015. **1**(4) DOI: 10.1099/mgen.0.000033.
88. Ralph, B. and D.C. Sheppard, *A Murine Model for Chronic A. fumigatus Airway Infections*, in *Host-Fungal Interactions*. 2021. p. 215-224.
89. Amos, B., et al., *VEuPathDB: the eukaryotic pathogen, vector and host bioinformatics resource center.* Nucleic Acids Research, 2022. **50**(D1): p. D898-D911 DOI: 10.1093/nar/gkab929.
90. Cherinka, B., et al., *Marvin: A Tool Kit for Streamlined Access and Visualization of the SDSS-IV MaNGA Data Set.* The Astronomical Journal, 2019. **158**(2) DOI: 10.3847/1538-3881/ab2634.
91. Haberthür, U. and A. Caflisch, *FACTS: Fast analytical continuum treatment of solvation.* Journal of Computational Chemistry, 2007. **29**(5): p. 701-715 DOI: 10.1002/jcc.20832.

951 **SUPPLEMENTARY FILES**

952 **Table S1**: Genes included in the NanoString custom codeset.

953 **Table S2**: *In vitro* and *in vivo* conditions assayed for the NanoString run.

954 **Table S3**: Primers employed in this study.

955 **Supplementary File 1**: NanoString designed Probes A and B for hybridisation and MTE primers for
956 enrichment.

957 **Supplementary File 2**: Raw data from digital analysis of hybridised codesets.

958 **Supplementary File 3:** Normalized data used for the analyses.